J. Fluid Mech. (2001), *vol.* 445, *pp.* 345–375. © 2001 Cambridge University Press
DOI: 10.1017/S002211200100564X Printed in the United Kingdom

Sensitive enhanced diffusivities for flows with fluctuating mean winds: a two-parameter study

By JAMES BONN AND RICHARD M. McLAUGHLIN

Department of Mathematics, University of North Carolina, Chapel Hill, NC 27599, USA
e-mail: bonn@amath.unc.edu; rmm@amath.unc.edu

(Received 29 September 2000 and in revised form 14 February 2001)

Enhanced diffusion coefficients arising from the theory of periodic homogenized averaging for a passive scalar diffusing in the presence of a large-scale, fluctuating mean wind superimposed upon a small-scale, steady flow with non-trivial topology are studied. The purpose of the study is to assess how the extreme sensitivity of enhanced diffusion coefficients to small variations in large-scale flow parameters previously exhibited for steady flows in two spatial dimensions is modified by either the presence of temporal fluctuation, or the consideration of fully three-dimensional steady flow. We observe the various mixing parameters (Péclet, Strouhal and periodic Péclet numbers) and related non-dimensionalizations. We document non-monotonic Péclet number dependence in the enhanced diffusivities, and address how this behaviour is camouflaged with certain non-dimensional groups. For asymptotically large Strouhal number at fixed, bounded Péclet number, we establish that rapid wind fluctuations do not modify the steady theory, whereas for asymptotically small Strouhal number the enhanced diffusion coefficients are shown to be represented as an average over the steady geometry. The more difficult case of large Péclet number is considered numerically through the use of a conjugate gradient algorithm. We consider Péclet-number-dependent Strouhal numbers, $S = Q\,Pe^{-(1+\gamma)}$, and present numerical evidence documenting critical values of γ which distinguish the enhanced diffusivities as arising simply from steady theory ($\gamma < -1$) for which fluctuation provides no averaging, fully unsteady theory ($\gamma \in (-1, 0)$) with closure coefficients plagued by non-monotonic Péclet number dependence, and averaged steady theory ($\gamma > 0$). The transitional case with $\gamma = 0$ is examined in detail. Steady averaging is observed to agree well with the full simulations in this case for $Q \leqslant 1$, but fails for larger Q. For non-sheared flow, with $Q \leqslant 1$, weak temporal fluctuation in a large-scale wind is shown to reduce the sensitivity arising from the steady flow geometry; however, the degree of this reduction is itself strongly dependent upon the details of the imposed fluctuation. For more intense temporal fluctuation, strongly aligned orthogonal to the steady wind, time variation averages the sensitive scaling existing in the steady geometry, and the present study observes a Pe^1 scaling behaviour in the enhanced diffusion coefficients at moderately large Péclet number. Finally, we conclude with the numerical documentation of sensitive scaling behaviour (similar to the two-dimensional steady case) in fully three dimensional ABC flow.

https://doi.org/10.1017/S002211200100564X Published online by Cambridge University Press

1. Introduction

Perhaps the most important outstanding problem of modern theories for fluid dynamics is understanding the origin of small-scale fluid turbulence arising in large-scale fluid experiments, and the assessment of those small-scale fluctuations upon large-scale observables. Indeed, one need look no further than the example of a turbulent jet to appreciate this fact. Landau, in 1944 (Landau 1944; Batchelor 1967; Landau & Lifschitz 1987), presented a beautiful exact solution of the Navier–Stokes equations, the Landau jet, which possesses the interesting property that for large jet momentum, the jet angle is seen to vanish, scaling as $(\nu^2\rho/M)^{1/2}$, where ν, ρ are the respective fluid viscosity and density, and M measures the jet momentum. However, turbulent jets are readily observed to have a non-zero angle of roughly 25° at large Reynolds number (Landau & Lifschitz 1987). These seemingly different predictions are reconciled through observing that the laminar jet is unstable (to vortex instabilities, etc.). Be it for the lack of a complete theory for small-scale fluid turbulence, or be it for the inability to resolve the energy-containing scales of complicated fluid motion, turbulence modellers have elected to utilize turbulent mixing coefficients to attempt to parameterize turbulence, and its effects upon large-scale observables. In the context of jets, if the viscosity is replaced by a 'turbulent' viscosity, $\nu_T \approx \lambda_T(M/\rho)^{1/2}$, a non-zero jet angle is readily achieved. This is essentially a Prandtl mixing length argument, and demonstrates explicitly how turbulence closure modelling may yield a prediction for how small-scale turbulence may affect large-scale observables. Unfortunately, the mathematics supporting this natural procedure does not yet exist, at least in the context of the deterministic Navier–Stokes equations.

A natural problem for assessing the validity of such closure modelling is that of a diffusing passive scalar, with prescribed small-scale turbulence incorporated through a variable coefficient advection. While directly only an analogy to turbulent jets, the point in this context is to develop rigorous averaging theories for replacing the effect of such rapidly varying coefficients by effective diffusion coefficients. The utility of working with a passive scalar is that the dynamics are linear, though many essential difficulties (such as problems of closure) are explicitly retained. This problem is akin to providing rigorous justificiation of Prandtl mixing length arguments in the simpler context of a linear evolution involving variable coefficients. Such theory has been completely developed using the method of homogenized averaging, and rigorously predicts that indeed (in many circumstances, see discussion below) the effect of these small scales may be incorporated as an effective, though sometimes anamolous, diffusion coefficient, thereby justifying mixing length arguments (Bensoussan, Lions & Papanicolaou 1978; Moffatt 1983; McLaughlin, Papanicolaou & Pironneau 1985; Pomeau 1985; McCarty & Horsthemke 1988; Solomon & Gollub 1988; Koch & Brady 1989; Koch *et al.* 1989; Young, Pumir & Pomeau 1989; Crisanti *et al.* 1990; Majda 1990; Avellaneda & Majda 1991; Knobloch & Merryfield 1992; Brenner & Edwards 1993; Majda & McLaughlin 1993; Fannjiang & Papanicolaou 1994; McLaughlin 1998).

But there is an essential difficulty. What is the coupling constant, λ_T? How does the coupling constant depend upon the large-scale geometry? How does it depend upon the details of the small-scale turbulence? These questions are fundamental to developing a complete theory for fluid turbulence, for it is this coupling constant which essentially sets the large-scale observable, the jet angle.

Work of Koch *et al.* (1989), Majda & McLaughlin (1993), and McLaughlin (1998) has demonstrated that these difficulties may be inherent and unavoidable, at least in idealized passive scalar studies. This work established sensitive dependence in the effective diffusion coefficients upon fluid flow parameters for two-dimensional

https://doi.org/10.1017/S002211200100564X Published online by Cambridge University Press

steady periodic flow with a mean wind (first formally by Koch *et al.* 1989 and rigorously proven by Majda & McLaughlin 1993). Specifically, the enhanced diffusion coefficients as predicted by homogenized averaging were shown rigorously to possess a discontinuity on a dense set of mean flow directions in the limit of infinite Péclet number, Pe, whereby the magnitude of the enhanced diffusion coefficient is seen to take $O(1)$ values for mean wind angles with irrational tangents, and $O(Pe^2)$ for angles with rational tangents (Majda & McLaughlin 1993) (see also related work of Fannjiang & Papanicolaou 1994). This surprisingly sensitive behaviour was further established numerically within the context of the infinite time homogenization theory to be present at finite Péclet number. This was established through the observance of sensitivity in the complicated crossover behaviour connecting the generically Pe^2 scaling at small Péclet number with the limiting behaviour at infinite Péclet number. It was documented that a small change, $\Delta \boldsymbol{V}$, in the large-scale steady mean wind leads to a dramatic change in large Pe scaling. Specifically, it was shown that a small change in a flow parameter caused the high Pe scaling of the enhanced diffusions to switch from $O(Pe^2)$ scaling to $O(1)$ scaling over a wide range of Péclet numbers (Koch *et al.* 1989; Majda & McLaughlin 1993). Moreover, using carefully benchmarked Monte-Carlo simulation, McLaughlin demonstrated that the sensitivity (to mean wind direction) in this crossover behaviour is observable at finite time (McLaughlin 1998), thereby showing that this sensitive scaling is not an artifact of the homogenization method. It should be observed that Avellaneda & Majda (1991) have proved that these two distinct scaling behaviours are the respective maximal and minimal Péclet scalings possible in this context. A very small change in a large-scale flow parameter produces dramatically different mixing properties of the passive scalar. As such, the natural interpretation of these sorts of results is that while the ideas of turbulent closure are well founded and rigorously justifiable, the empirical task of determining the precise closure coefficients may suffer from intrinsic difficulties.

The natural question to ask is how the addition of time variation into the fluid motion, or the consideration of three-dimensional, as opposed to two-dimensional flow may somehow alter these sensitive predictions in the steady, or two-dimensional geometry. Some necessary ergodic conditions have been developed to guarantee when a time-dependent flow will induce maximal Péclet number scaling, Pe^2 (Mezic, Brady & Wiggins 1996), but much less is known generally (specifically, for ergodic flows), especially regarding the determination of the asymptotic scaling properties for ergodic flows. Certainly, the hope is that strong temporal fluctuation will in some way smooth the poor, and sensitive scaling behaviour arising in the steady geometry. Of course, the addition of temporal fluctuation adds considerable complexity, and in the light of the complex behaviour already present in the steady geometry, a complete theoretical description of how time variation modifies the effective mixing seems extremely difficult. Consequently, it is the purpose of this paper to carefully explore these issues through the careful asymptotic and numerical calculation of enhanced eddy diffusion coefficients arising from mathematical theories of homogenized averaging.

Here, we study the enhanced diffusion coefficients which arise out of the theory of homogenized averaging for two-dimensional periodic flows involving *unsteady* mean winds, and three-dimensional steady (ABC) flows through use of a carefully benchmarked conjugate gradient algorithm along with asymptotic consideration of a variety of limiting cases. We present a brief review of previous studies of these homogenized effective diffusion coefficients and their sensitive flow parameter dependence. We additionally discuss the various non-dimensionalizations and parameters (Péclet, periodic Péclet, Strouhal numbers) possible for spatio-temporal advections,

https://doi.org/10.1017/S002211200100564X Published online by Cambridge University Press

and address subtle differences in parametric dependences. At fixed, bounded Péclet numbers, the limiting cases of asymptotically small and large Strouhal numbers (or equivalently large and small periodic Péclet numbers, respectively) are shown to be reduced to steady theory. We show that the former case is given by a temporal average over the enhanced diffusion coefficients arising in the steady geometry with *frozen* temporal coefficient, while the latter case agrees precisely with the steady geometry, with the temporal velocity fluctuation replaced by its time average.

The more difficult case involving high Péclet numbers is explored utilizing a conjugate gradient algorithm to integrate the associated time-varying cell problem. This algorithm is carefully benchmarked using the time-varying shear layer (Majda & Kramer 1999). We document that the phenomenon varies greatly with Strouhal number, and consider the Péclet-number-dependent Strouhal numbers, $S = Q\,Pe^{-(1+\gamma)}$, for constant Q. For cases with $\gamma > 0$, we compare the full numerical solution of the temporally varying cell problem with that of a straight average over the steady geometry. This comparison shows that steady averaging over frozen temporal coefficients provides an excellent approximation to the fully time-dependent cell problem, as might be expected through formal arguments at *fixed* Péclet number. In this regime, temporal fluctuation in fact provides enough averaging to smooth the sensitive parameter dependence which occurs for steady flows. Here, we numerically observe a Pe^1 scaling law for strong enough fluctuations over a range of Péclet numbers. However, for cases with $\gamma \in (-1, 0)$, steady averaging fails, and full simulation of the temporally varying cell problem is required for accurate coefficient tabulation. In these cases, the enhanced diffusion coefficients are observed to exhibit complicated non-monotonic Péclet number dependence. This behaviour is discussed with regard to known Stieltjes measure formulas existing for temporally fluctuating flows (Avellaneda & Vergassola 1995). For $\gamma \leqslant -1$, the temporal fluctuation is irrelevant as the coefficients are observed to be governed in this regime by the steady theory. For cases with $\gamma < 0$, there is little hope for temporal fluctuation to massage the troubling predictions of the steady geometry.

Lastly, we show that sensitive scaling behaviour is not an artifact of two-dimensional steady flow by explicitly documenting that, in steady ABC flow, the enhanced diffusion coefficients may experience sensitive Péclet number scaling behaviour similar to that occurring in the two-dimensional case.

2. Scaling and non-dimensional mixing parameters

To begin, we consider the passive scalar equation in dimensional form, and discuss the different non-dimensional parameters which may be identified to assist in identifying transport properties. Let T be the concentration of a scalar diffusing in the presence of a prescribed velocity field. T satisfies the following evolution equation:

$$\frac{\partial T}{\partial t} + \boldsymbol{u} \cdot \nabla T = \kappa \Delta T. \tag{2.1}$$

Here, κ is the tracer's molecular diffusivity, and the incompressible velocity field $\boldsymbol{u}$ is spatially periodic with period L (assumed for brevity in exposition to be the same in all directions), and temporally periodic with time period T_P. Let $\bar{V}$ denote a characteristic velocity field. From the dimensional parameters, $\bar{V}, \kappa, L, T_P$, we may form three non-dimensional parameters, the Strouhal number, $S = L/(T_P \bar{V})$, the Péclet number, $Pe = \bar{V}L/\kappa$, and the periodic Péclet number, $\tau_P = \kappa T_P / L^2$. The Péclet number measures the relative strength of fluid advection to molecular diffusion, while the Strouhal and periodic Péclet numbers are ratios of time scales, Strouhal being

https://doi.org/10.1017/S002211200100564X Published online by Cambridge University Press

the ratio of the characteristic velocity sweeping time to period time, and the periodic Péclet measuring the ratio of the time period to the diffusion time. These parameters are not independent, but in fact are algebraically related through

$$\tau_P = \frac{1}{S\,Pe}. \tag{2.2}$$

Consequently, there are different non-dimensionalizations possible with these parameters. In this paper, we are particularly interested in studying how temporal fluctuation affects Péclet number scalings on long, diffusive time scales, and as such we will primarily consider the parameterizations: (Pe, τ_P). To this end, let $\boldsymbol{y} = \boldsymbol{x}/L$, $\tau = t\kappa/L^2$, and $\boldsymbol{v} = \boldsymbol{u}/\bar{V}$. In these new non-dimensional variables, the passive scalar evolves according to

$$\frac{\partial T}{\partial \tau} + Pe\,\boldsymbol{v}(\boldsymbol{y}, \tau) \cdot \nabla T = \Delta T. \tag{2.3}$$

The flow field in this non-dimensionalization has unit spatial period, and temporal period τ_P.

Observe that an alternative non-dimensionalization is possible in which $\boldsymbol{y} = \boldsymbol{x}/L$, $\tau = t/T_P$, and $\boldsymbol{v} = \boldsymbol{u}/\bar{V}$. In this non-dimensionalization, the passive scalar evolves as

$$Pe\left(S\frac{\partial T}{\partial \tau} + \boldsymbol{v} \cdot \nabla T\right) = \Delta T$$

where $\boldsymbol{v}$ has unit periods in both space and time. Avellaneda & Vergassola (1995) generalized earlier work for steady flow (Avellaneda & Majda 1991) to temporally varying flows to show that the enhanced diffusivities arising in homogenized averaging (see § 3.1 below) in fact may be represented through a Stieltjes measure formula in this *particular* non-dimensionalization. One ramification of this observation is that the ensuing effective mixing coefficients should be expected to demonstrate monotonic dependence in the Péclet number at fixed Strouhal number. We point out that in the previous non-dimensionalization, such a representation is not guaranteed. In fact, we document below non-monotone Péclet number behaviour in a time-varying shear layer at fixed (small) periodic Péclet numbers, τ_P. We demonstrate below that this non-monotone behaviour is consistent with the Stieltjes measure formula through the nonlinear algebraic identity (2.2), and emphasize that these differences reflect the different time scales studied in these two distinct non-dimensionalizations. More complete discussion of these subtleties regarding the mixing properties for passive transport with temporally varying flows will be given at the end of the following section.

We further comment that with the algebraic parameter relation given in (2.2), studying the mixing properties for flows with large Péclet number and fixed periodic Péclet number yields the indirect consideration of the vanishing Strouhal number singular limit: $S = 1/(Pe\,\tau_P) \to 0$. It is in this limit that several authors have identified the possibility of interesting non-universal behaviour (Castiglione 2000; Ottaviani 1992). Below, we explore in great detail this limit, as well as others.

3. Previous theory and results

3.1. *Homogenization for temporally varying flows*

Employing standard methods of homogenized averaging (Bensoussan *et al.* 1978; McLaughlin *et al.* 1985; Majda & Kramer 1999), we consider the space–time averaging of the passive scalar equation given in (2.3) with a periodic velocity field with unit

https://doi.org/10.1017/S002211200100564X Published online by Cambridge University Press

spatial periods, and temporal period τ_P. A separation of scales is introduced through the assumption of a slowly varying initial temperature field, $T|_{t=0} = T_0(\delta \boldsymbol{y})$. Define the spatio-temporal average to be

$$\langle \cdot \rangle \equiv \frac{1}{\tau_P} \int_{[0,\tau_P]} \int_{[0,1]^d} \cdot \, \mathrm{d}\boldsymbol{x} \, \mathrm{d}t \tag{3.1}$$

with d the spatial dimension of the velocity. We separate the periodic velocity field into its mean, $\boldsymbol{V}$, and mean free, $\boldsymbol{v}$, $\langle \boldsymbol{v} \rangle = 0$ components. Then, making the usual long-time, parabolic rescaling of space–time, the problem to average is

$$\frac{\partial T^{(\delta)}}{\partial t} + \delta^{-1} Pe \left(\boldsymbol{v}\left(\frac{\boldsymbol{x}}{\delta}, \frac{t}{\delta^2} \right) + \boldsymbol{V} \right) \cdot \nabla T^{(\delta)} = \Delta T^{(\delta)}, \tag{3.2}$$

$$T^{(\delta)}(\boldsymbol{x}, 0) = T_0(\boldsymbol{x}).$$

The limit of vanishing δ has been well studied by homogenization theory. We summarize the results of this averaging procedure and direct the reader to the literature for details regarding this calculation (Bensoussan *et al.* 1978; McLaughlin *et al.* 1985; Majda 1990; McLaughlin 1994; Majda & Kramer 1999). In a frame of reference moving with the mean wind, $\boldsymbol{V}$, the renormalized passive scalar equation in the limit of vanishing δ is seen to satisfy the effective diffusion equation:

$$\frac{\partial \bar{T}(\boldsymbol{x}, t)}{\partial t} = \nabla \cdot (\bar{\boldsymbol{K}} \nabla \bar{T}(\boldsymbol{x}, t)) \tag{3.3}$$

$$\bar{T}(\boldsymbol{x}, 0) = T_0(\boldsymbol{x}),$$

where $\bar{\boldsymbol{K}} = (\boldsymbol{I} + \boldsymbol{\kappa})$. The tensor $\boldsymbol{\kappa}$ is defined as

$$\boldsymbol{\kappa}_{i,j} = \langle \nabla \Theta_i \cdot \nabla \Theta_j \rangle \tag{3.4}$$

for $i, j = 1, \ldots, d$, where $\langle \cdot \rangle$ is the spatial and time average that we defined in (3.1). This tensor represents the addition to the diffusion tensor of the original advection–diffusion equation resulting from the effect of the background velocity, and is denoted the enhanced diffusion tensor. The new term, Θ_j, is the unique, mean zero solution of the periodic boundary value (cell) problem

$$\frac{\partial \Theta_j(\boldsymbol{x}, t)}{\partial t} - \Delta \Theta_j(\boldsymbol{x}, t) + Pe(\boldsymbol{v}(\boldsymbol{x}, t) + \boldsymbol{V}) \cdot \nabla \Theta_j(\boldsymbol{x}, t) = -Pe \, v_j(\boldsymbol{x}, t). \tag{3.5}$$

Here, v_j denotes the jth component of the mean free portion of the velocity field. It should be noted that the boundary conditions for this problem are periodic in both space and time (with unit period in space, and temporal period τ_P in this particular non-dimensionalization), and as such the problem does not have an initial condition. Instead, the solution $\Theta_j(\boldsymbol{x}, t)$ has the same periodicity as the driver, $v_j(\boldsymbol{x}, t)$. The uniqueness of the solution in this framework has been established in the literature (Bensoussan *et al.* 1978; Majda 1990; Majda & Kramer 1999). Attempts have been made to study the temporally varying cell problem for cases where the velocity field admits fluctuations (Castiglione *et al.* 1998; Castiglione 2000), using time stepping. The algorithm we develop below does not utilize time stepping, but instead forces the proper boundary condition through a full spatio-temporal spectral decomposition.

Previous mathematical studies have shown that enhanced diffusion coefficients given by the inner product in (3.4) may be represented (for the second non-dimensionalization with group (Pe, S)) in terms of a Stieltjes measure formula quite

https://doi.org/10.1017/S002211200100564X Published online by Cambridge University Press

generally (Avellaneda & Majda 1991; Avellaneda & Vergassola 1995):

$$\bar{K} = 1 + Pe^2 \int \frac{\sigma(\mathrm{d}\lambda, S)}{1 + Pe^2\,\lambda^2}. \tag{3.6}$$

Here, σ represents some (unknown) measure which depends upon the Strouhal number. Stieltjes measure formulae are useful in many regards, specifically in deducing rigorous bounds for the enhanced diffusivities as a function of Péclet number (Avellaneda & Majda 1991; Majda & McLaughlin 1993; Fannjiang & Papanicolaou 1994). Further, these formulae additionally imply monontonic dependence in the Péclet number, at fixed Strouhal number. It should be stressed that this conclusion is somewhat misleading: for Péclet-number-dependent Strouhal numbers, $S = S(Pe)$, the measure itself implicitly admits Péclet number dependence, and all monotonicity may be lost. Indeed, we demonstrate explicitly below in § 6 conditions under which monotone Péclet number dependence is lost.

3.2. *Previous results with a Childress–Soward flow*

In previous work, Majda & McLaughlin (1993), and McLaughlin (1998), using a variety of rigorous elliptic theory, computational study of the elliptic cell problem, and Monte-Carlo simulations for the Brownian trajectories underlying the dynamic passive scalar equation, carefully documented that the Péclet number scaling would be sensitively dependent upon flow parameters for steady fluid flows possessing a mean wind. Specifically, they considered the fluid flow given by the following Childress and Soward streamfunction:

$$\psi_{steady} = \sin(2\pi x)\sin(2\pi y) + \varepsilon\cos(2\pi x)\cos(2\pi y) \tag{3.7}$$

where $0 \leqslant \varepsilon \leqslant 1$. They established that the enhanced diffusivity tensor would show dramatically different scaling behaviour for small changes in the angle of the large-scale mean wind, $\boldsymbol{V} = (V_x, V_y)^t$. Rigorous theory documents that in the limit of infinite Péclet number, the enhanced diffusivities possess a discontinuity on a dense set of mean wind angles whereby the enhanced diffusion switches from the asymptotic Pe^2 scaling for winds whose angles possess rational tangents, to $O(1)$ scaling for irrational tangents (Majda & McLaughlin 1993; Fannjiang & Papanicolaou 1994). At finite Péclet number, similar behaviour was documented through computational study of the elliptic cell problem. Numerically, the enhanced diffusion coefficients were seen to exhibit a dramatic change in scaling for small perturbations in the mean wind (Koch *et al.* 1989; Majda & McLaughlin 1993). McLaughlin (1998) demonstrated using carefully benchmarked Monte-Carlo simulation of the underlying stochastic trajectories that this sensitive scaling is not an artifact of the homogenized averaging of the passive scalar equation, but in fact is intrinsic to the system. Figure 1 illustrates the typical behaviour (the same as studied by McLaughlin 1998, similar to studies performed in Majda & McLaughlin 1993). Shown is a log-log plot of the enhanced diffusion coefficient $\kappa_{1,1}$ as a function of Péclet number, obtained as a numerical solution of the elliptic cell problem, for the Childress–Soward flow above with representative parameter, $\varepsilon = 0.5$, for two slightly different mean winds. The top curve corresponds a mean wind $\boldsymbol{V} = (-15, 15)$, while the bottom curve corresponds to $\boldsymbol{V} = (-15.5, 15)$. Observe that the small change in the mean wind is essentially not noticeable at small Péclet numbers as the curves are indistinguishable, but at a Péclet number $Pe \approx 10$, the two curves dramatically 'split'. It should be emphasized that this splitting covers the *full* range of rigorously allowable Péclet number scalings, with the upper case following Pe^2, and the bottom case following Pe^0. To summarize, a

https://doi.org/10.1017/S002211200100564X Published online by Cambridge University Press

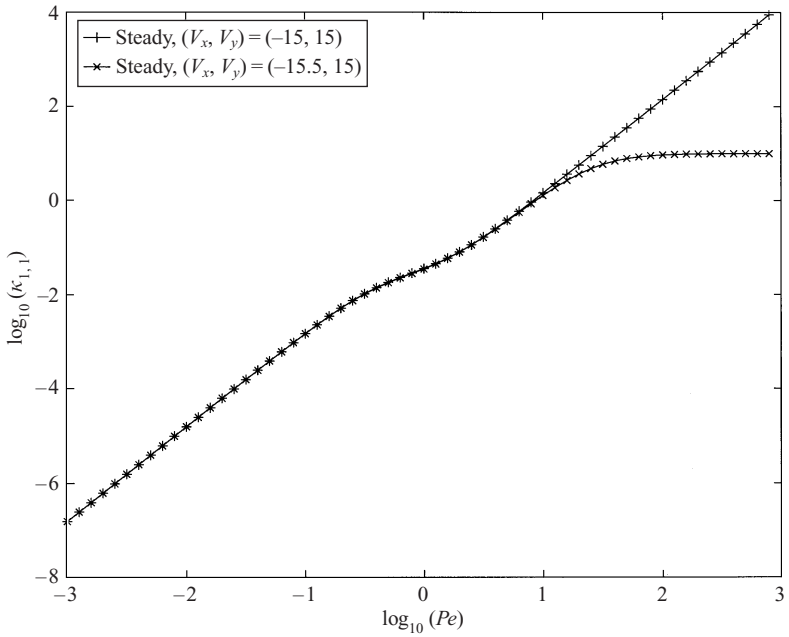


FIGURE 1. Re-creation of the splitting first seen in McLaughlin (1998) for the steady flow derived from the Childress–Soward streamfunction. For both curves, $\varepsilon = 0.5$. Notice that the small change in mean wind can create a dramatic difference in the Péclet number scaling of the enhanced diffusion.

small perturbation, $\Delta \boldsymbol{V} = (0.5, 0)$, in the large-scale steady wind produces a dramatic change in Péclet scaling at moderately large Péclet numbers.

Two issues are apparent. First, how does the addition of time variation into the mean wind modify this splitting which is indicative of extremely sensitive Péclet number scaling. And second, can this complicated splitting occur in a fully three-dimensional flow.

4. Numerical technique

Here, we outline the conjugate gradient algorithm used to numerically solve the time-varying cell problem given in (3.5). We will consider two different types of velocity fields. First, we explore temporal generalizations of the two-dimensional steady Childress–Soward flows considered by Majda and McLaughlin (Majda & McLaughlin 1993; McLaughlin 1998). Secondly, we consider fully three-dimensional steady ABC flow. Below, we explain in full detail the methodology employed for the unsteady two-dimensional flow, and observe that the methodology is quite similar for the case of the three-dimensional ABC flow. Additional details may be obtained from Bonn (2001).

4.1. *Numerical discretization*

Here, we document the numerical algorithm utililized to solve the cell problem given in (3.5). We consider solutions of the cell problem for velocity fields obtained by adding a time-dependent perturbation to the flow given by the steady, mean free

https://doi.org/10.1017/S002211200100564X Published online by Cambridge University Press

Childress–Soward streamfunction. Specifically, we consider velocities of the form $\boldsymbol{v}(\boldsymbol{x},t) = \boldsymbol{v}(\boldsymbol{x}) + \boldsymbol{A}(t)$ where

$$\left.\begin{aligned} \boldsymbol{v}(\boldsymbol{x}) &= \nabla^{\perp}(\sin(2\pi x)\sin(2\pi y) + \varepsilon\cos(2\pi x)\cos(2\pi y)), \\ \boldsymbol{A}(t) &= \begin{pmatrix} \delta_x \sin\left(\dfrac{2\pi}{\tau_P}t\right) \\ \delta_y \sin\left(\dfrac{2N\pi}{\tau_P}t + \phi\right) \end{pmatrix}, \end{aligned}\right\} \tag{4.1}$$

where ϕ is a constant phase, N is an integer which allows for different (commensurate) rates of fluctuation between the horizontal and vertical wind fields, and the perpendicular gradient operator is defined as $\nabla^{\perp} = (\partial/\partial y, -\partial/\partial x)^t$. The constant mean velocity is given by $\boldsymbol{V} = (V_x, V_y)^t$, so that the full velocity field studied below is $\boldsymbol{V} + \boldsymbol{v}(\boldsymbol{x},t)$. Notice that the spatial period of the velocity is 1 and time period is τ_P. Also notice that the mean of the velocity field, $\boldsymbol{v}(\boldsymbol{x},t)$, is zero. We are primarily interested in exploring how the presence of temporal fluctuation, here taken to be a low-mode simple sinusoidal fluctuation, affects the complicated Péclet number splitting behaviour occurring as the steady mean wind is perturbed. In this study, the parameters adjusting the flow's unsteadiness are the intensities, (δ_x, δ_y), and the time period, τ_P (or Strouhal number, S).

We next document the numerical discretization employed and the conjugate gradient iteration scheme utilized to invert the system. The reader not interested in the details of the numerical algorithm may skip ahead to § 5.

To arrive at the unique mean zero solution, we follow the example of Majda & McLaughlin (1993) and use a Fourier spectral method. Specifically, we let

$$\Theta_j = \sum_{l,m,n\neq 0} A^j_{n,m,l} \exp\left(2\pi\mathrm{i}\left(nx + my + \frac{l}{\tau_P}t\right)\right),$$

$$v_j = \sum_{l,m,n\neq 0} \hat{v}^j_{n,m,l} \exp\left(2\pi\mathrm{i}\left(nx + my + \frac{l}{\tau_P}t\right)\right).$$

Substituting these and taking the convolution, we obtain the following infinite system of linear equations for the spectral coefficients $A^j_{n,m,l}$ (Bonn 2001):

$$\begin{aligned} &\zeta_{n,m}A^j_{n,m,l-N} + \rho_{n,m}A^j_{n,m,l-1} + \beta_{n,m}A^j_{n-1,m-1,l} \\ &\quad + \gamma_{n,m}A^j_{n+1,m-1,l} + \alpha'_{n,m,l}A^j_{n,m,l} - \gamma_{n,m}A^j_{n-1,m+1,l} \\ &\quad - \beta_{n,m}A^j_{n+1,m+1,l} - \rho_{n,m}A^j_{n,m,l+1} - \zeta^*_{n,m}A^j_{n,m,l+N} = -Pe\,\hat{v}^j_{n,m,l} \end{aligned} \tag{4.2}$$

where the superscript asterisk means the complex conjugate. The coefficients are defined as follows:

$$\left.\begin{aligned} \alpha'_{n,m,l} &= \alpha_{n,m} + 2\pi\mathrm{i}\left[\frac{l}{\tau_P} + Pe(V_x n + V_y m)\right], \quad \alpha_{n,m} = 4\pi^2(n^2+m^2), \\ \beta_{n,m} &= \pi^2 Pe\,(1-\varepsilon)(n-m), \quad \gamma_{n,m} = -\pi^2 Pe\,(1+\varepsilon)(n+m), \\ \rho_{n,m} &= \pi\, Pe\,\delta_x n, \quad \zeta_{n,m} = \pi\, Pe\,\delta_y m(\cos(\phi) + \mathrm{i}\sin(\phi)), \end{aligned}\right\} \tag{4.3}$$

where we have used the known spectral coefficients of the velocity field. Note that

https://doi.org/10.1017/S0022112001005564X Published online by Cambridge University Press

reality of the solution requires that $(A^j_{n,m,l})^* = A^j_{-n,-m,-l}$. This relation follows from conjugating (4.2) and noticing that the same result follows from replacing the index triplet (n,m,l) with $(-n,-m,-l)$.

To solve this infinite-dimensional system, we must truncate it to a system of finite size, limiting the Fourier modes to $n,m,l = -M,\ldots,M$. Now we have a linear system of $(2M+1)^3$ equations and unknowns. However, the known Fourier representation of the velocity field (the driver) allows us to decouple the system into two parts, where $n+m$ is odd and where $n+m$ is even. The part with $n+m$ odd is a homogenous system of equations, and thus the solution of this part is $A^j_{n,m,l} = 0$ for $j = 1,\ldots,d$ and $n,m,l = -M,\ldots,M$. Further notice that the Fourier mode $A^j_{0,0,0}$ has been excluded from the equations by our definition of the spectral expansion of Θ_j. To treat this correctly, to obtain a mean zero solution, we set $A^j_{0,0,0} = 0$. Lastly, observe that the part of the system where $n = m = 0$ is diagonal. This portion of the system is inverted first and subsequently utilized to complete the inversion.

Once the solution is obtained, the enhanced diffusion coefficient $\kappa_{1,1}$, is calculated with the aid of the the identity $\langle \nabla\Theta_i \cdot \nabla\Theta_j \rangle = -Pe\langle v_i\Theta_j + v_j\Theta_i\rangle/2$. Using the calculated solution $A^j_{n,m,l}$ and the spectral form of $\boldsymbol{v}$, the enhanced diffusion coefficient can be written as

$$\kappa_{1,1} = Pe\,(\pi[(1-\varepsilon)\,\mathrm{Im}\,(A^1_{1,1,0}) + (1+\varepsilon)\,\mathrm{Im}\,(A^1_{1,-1,0})] + \delta_x\,\mathrm{Im}\,(A^1_{0,0,1})).$$

To verify convergence of this approach to solutions of the limiting infinite-dimensional system, M is increased to ensure that enough spectral modes are retained to accurately describe the solution to the cell problem. The criterion employed to determine convergence is based upon the relative difference between the enhanced diffusions calculated at successive values of M. We declare a simulation to be converged at a particular Péclet number if this relative difference is less than a given tolerance. In the simulations discussed below, this tolerance was selected to be 10^{-3}.

As mentioned above, when discretizing the cell problem arising from the ABC flow, the process is similar. The system does not decouple as nicely; however, the basic ideas are the same (Bonn 2001).

4.2. *Conjugate gradient iteration scheme*

Here we discuss the iterative method utilized to obtain solutions of the finite-dimensional problem given above in (4.2).

The system of equations has been reduced to the linear system $\boldsymbol{B}\boldsymbol{A}^j = -Pe\,\hat{\boldsymbol{v}}^j$. The matrix $\boldsymbol{B}$ has a special stucture, it can be written as $\boldsymbol{B} = \boldsymbol{D} + \boldsymbol{C}$ where $\boldsymbol{D}$ is a diagonal matrix with real, positive elements which are independent of the Péclet number, and $\boldsymbol{C}$ is skew Hermitian, $\boldsymbol{C}^H = -\boldsymbol{C}$, where $\boldsymbol{C}^H$ means the conjugate transpose. With the structure of $\boldsymbol{D}$, there exists an invertible matrix $\boldsymbol{D}^{1/2}$ where $\boldsymbol{D} = \boldsymbol{D}^{1/2}\boldsymbol{D}^{1/2}$. Thus $\boldsymbol{D}^{-1/2}\boldsymbol{B}\boldsymbol{D}^{-1/2} = \boldsymbol{I} + \boldsymbol{F}$ where $\boldsymbol{F} = \boldsymbol{D}^{-1/2}\boldsymbol{C}\boldsymbol{D}^{-1/2}$. Notice that $\boldsymbol{F}$ is also a skew Hermitian matrix since $\boldsymbol{D}$, and thus $\boldsymbol{D}^{-1/2}$, are diagonal matrices. Therefore, the system $\boldsymbol{B}A^j = -Pe\,\hat{\boldsymbol{v}}^j$ is equivalent to the system $(\boldsymbol{I}+\boldsymbol{F})\boldsymbol{x} = \boldsymbol{b}$ where $A^j = \boldsymbol{D}^{-1/2}\boldsymbol{x}$ and $\boldsymbol{b} = -Pe\,\boldsymbol{D}^{-1/2}\hat{\boldsymbol{v}}^j$.

The eigenvalues of this system, μ, all have real part, $\mathrm{Re}\,(\mu) = 1$. This is a result of the fact that the eigenvalues of the skew Hermitian matrix $\boldsymbol{F}$ are purely complex. Therefore, the eigenvalues of $\boldsymbol{I}+\boldsymbol{F}$ are just those of $\boldsymbol{F}$ shifted to the right by 1. Thus, the linear system is obviously invertible.

To solve the system $(\boldsymbol{I}+\boldsymbol{F})\boldsymbol{x} = \boldsymbol{b}$ where $\boldsymbol{F}$ is skew Hermitian, we use a conjugate gradient scheme developed by Concus & Golub (1976). The idea is to use an iterative

https://doi.org/10.1017/S002211200100564X Published online by Cambridge University Press

Péclet number	M	Size of system, $(2M+1)^3$	Number of iterations for convergence
10^{-3}	5	1331	2
10^{0}	5	1331	28
10^{1}	5	1331	235
$10^{1.5}$	6	2197	781
10^{2}	27	166 375	2653
$10^{2.4}$	52	1157 625	5777

TABLE 1. Number of iterations needed for the conjugate gradient method with no preconditioning to converge for the case $\delta_x = \delta_y = 0.65$ and $N = 1$ where the mean wind is $(V_x, V_y)^t = (-15, 15)^t$.

scheme of the type

$$\boldsymbol{x}^{k+1} = \boldsymbol{x}^{k-1} + \omega_{k+1}(v_k \boldsymbol{r}^k + \boldsymbol{x}^k - \boldsymbol{x}^{k-1})$$

where $\boldsymbol{r}^k$ is the residual after the kth step, $\boldsymbol{r}^k = \boldsymbol{b} - (\boldsymbol{I} + \boldsymbol{F})\boldsymbol{x}^k$. The coefficients ω_{k+1} and v_k are chosen so that the residuals at all steps are conjugate to each other, i.e. $(\boldsymbol{r}^j)^H \boldsymbol{r}^k = 0$ when $j \neq k$. We find that the condition for conjugacy of residuals is

$$v_k = \frac{(\boldsymbol{r}^k)^H \boldsymbol{r}^k}{(\boldsymbol{r}^k)^H \boldsymbol{r}^k + (\boldsymbol{r}^k)^H \boldsymbol{F}\, \boldsymbol{r}^k} \quad \text{and} \quad \omega_{k+1} = \frac{(\boldsymbol{r}^{k-1})^H \boldsymbol{r}^{k-1}}{(\boldsymbol{r}^{k-1})^H \boldsymbol{r}^{k-1} + \left(\dfrac{v_k}{\omega_k^* v_{k-1}^*}\right)(\boldsymbol{r}^k)^H \boldsymbol{r}^k}.$$

Our iterative convergence criterion is based upon residuals. We say there is convergence to a solution for a particular M when the ratio of the size of the residual to the original right-hand side is less than some prescribed tolerance, or

$$\frac{\|\boldsymbol{r}^k\|_2}{\|\boldsymbol{b}\|_2} < \text{tolerance}.$$

The tolerance used to determine convergence of the iteration scheme, with M modes, is 10^{-8} in all simulations discussed below. We also tried checking for convergence when the computed enhanced diffusion coefficient, as opposed to the residual, met a similar criterion. The results were not significantly different. In table 1, we document the number of iterations needed to converge for a few values of M for the choice of parameters $\delta_x = \delta_y = 0.65$, the mean wind $(V_x, V_y)^t = (-15, 15)^t$, and $N = 1$. Observe that even though higher Péclet numbers required utilizing additional Fourier modes (larger M), the number of iterations needed to converge to the solution for each particular M is typically much less than the size of the system, $(2M+1)^3$. This scheme was performed without preconditioning which, looking at the convergence results, is acceptable.

5. Benchmarks

5.1. *Reproducing steady behaviour*

The first benchmark of our numerical technique is to reproduce the steady-state behaviour found by McLaughlin (1998). This was done by setting $\delta_x = \delta_y = 0$ and the results were shown in figure 1 which duplicates the original splitting observed by McLaughlin using direct inversion of a banded matrix, here derived using the conjugate gradient algorithm outlined above. A few remarks are in order regarding comparative timings and memory usage for the direct banded algorithm and the

https://doi.org/10.1017/S002211200100564X Published online by Cambridge University Press

conjugate gradient algorithm employed here. In the case of steady flow, the system is two-dimensional. This means that the resulting matrix system is comparatively small. As a result, the direct method of using a banded solver is faster than using the conjugate gradient iteration scheme. This is reported by timing results of simulations run with the parameters $\varepsilon = 0$, $V_x = V_y = 0$ and finding the enhanced diffusion coefficients for the values of the Péclet number where $\log_{10}(Pe)$ runs from -3 to 2.9 in steps of 0.1 (60 values). The simulations were performed on a Compaq AlphaServer DEC21000 with a 525 Mhz processor. The wall clock time for the banded direct solver and the conjugate gradient algorithm are, respectively, 37.11 s and 329.07 s. The conjugate gradient algorithm takes approximately 9 times as long as the direct banded solver. As we change the problem from having a steady-state velocity to an unsteady velocity, since we have periodicity in time as well as space, we have a three-dimensional problem. The conjugate gradient algorithm does not require the formation of any matrices, only the ability to perform the matrix multiplication on a vector. The direct banded solver requires at least forming the part of the matrix between the outermost bands. In the three-dimensional problem, this becomes infeasible in terms of memory usage. Many of our simulations required an M, described above as the cutoff value of the Fourier modes used, of at least 50, and for three of the simulations, we verified convergence by using $M = 100$. The conjugate gradient algorithm uses memory on the order of M^3, while the direct banded solver would use memory on the order of M^5, since the band width of the system is on the order of M^2. While not fully optimized, our conjugate gradient code used slightly more than one gigabyte of memory on the simulation where $M = 100$; the direct banded solver would not be able to solve that problem with the memory available.

An additional remark should be made regarding the possibility of utilizing particle simulations of the stochastic differential equations underlying (2.3) to calculate effective diffusion coefficients. This approach, while limited by the slow convergence of the Monte-Carlo average, has been shown nonetheless to lead to quite accurate calculations of the enhanced diffusion coefficients (Crisanti *et al.* 1990; McLaughlin 1998). For the steady geometry explored here, McLaughlin (1998) has documented the success of this approach in observing the splitting in the Péclet number scaling shown in figure 1, thereby documenting the success of the homogenization theory at *finite time*. Of course, this approach, in the two-dimensional steady geometry, is computationally more expensive than the direct banded inversion. In the unsteady geometry, it is interesting to compare timing of the conjugate gradient algorithm with that of a particle simulation algorithm (not developed in this article). While the nature of the convergence of these algorithms is very different, we can nonetheless make a rough comparison. To obtain a single enhanced diffusion coefficient accurately using a modified version of the code employed by McLaughlin at $Pe = 56$, $V_x = -15.5$, $V_y = 15$, $\delta_y = 0.05$, $\delta_x = 0.1$, $N = 1$, $\phi = 0$, $\tau_P = 1$, requires approximately 40 minutes to one hour of wall clock time on the 525 Mhz Dec Alpha processor, while the same data point is obtained using the conjugate gradient algorithm in only 2.44 s. However, while timings for Monte-Carlo methods do not vary largely as δ_x and δ_y are increased, the conjugate gradient method does exhibit this tendency. Moreover, it should be noted that Monte-Carlo methods are less restricted by memory limitations which do pose serious limitations even for the present conjugate gradient algorithm. A simulation where $\delta_x = \delta_y = 0.5$ and $V_x = -15$, with the rest of the parameters unchanged, took approximately 95 s with the conjugate gradient algorithm. Also, as the Péclet number is increased, the time to resolve the enhanced diffusion coef-

https://doi.org/10.1017/S002211200100564X Published online by Cambridge University Press

ficient with the conjugate gradient technique also increases, as usually more Fourier modes are needed. This ultimately imposes a memory limitation upon exactly what can be computed. All things considered, the homogenization theory, coupled with a carefully benchmarked conjugate gradient method is certainly the most efficient and accurate of these algorithms, at least as regards obtaining the renormalized coefficients.

5.2. *Integral representations for the time-dependent shear flow*

The second benchmark we explore is the time-varying shear profile, introduced by Majda & Kramer (1999). This solution arises in the special case having the flow parameter $\varepsilon = 1$, for which an analytical solution is available which represents the enhanced diffusion coefficients in terms of an explicit integral (Majda & Kramer 1999). Also, P. R. Kramer (private research notes) derived an alternative integral formulation which is somewhat better conditioned for numerical quadrature. For these results in this subsection we set $N = 1$ and $\phi = 0$. We use numerical quadrature to calculate the integrals, providing a more stringent benchmark on which to validate the conjugate gradient algorithm.

Calculations of Majda & Kramer (1999) yielded an explicit infinite integral reprentation for the special case of a shear layer with a fluctuating transverse mean wind. The temporal boundary conditions were enforced through use of Duhamel's principle. Following this approach in the present geometry (essentially identical to Majda & Kramers' calculation, differing only to handle the rotated geometry considered here) yields the following infinite integral formula for the enhanced diffusion coefficient:

$$\kappa_{1,1} = \frac{2\pi^2 Pe^2}{\tau_P} \int_0^{\infty} \int_0^{\tau_P} \mathrm{e}^{-8\pi^2 u} \cos \left\{ 2\pi\, Pe[V_y - V_x]u \right. \\ \left. + \tau_P\, Pe(\delta_x - \delta_y) \left[\cos\left(\frac{2\pi}{\tau_P}\tau\right) - \cos\left(\frac{2\pi}{\tau_P}[\tau - u]\right) \right] \right\} \mathrm{d}\tau\, \mathrm{d}u. \quad (5.1)$$

Majda & Kramer (1999) utilized a similar representation to deduce the large Pe asymptotics at fixed τ_P (see discussion below). At fixed Pe, this integral requires numerical tabulation. We use two different approaches to obtain this benchmark. First, we utilize a two-dimensional Simpson's Rule created in *Matlab*. The infinite integral can be computed on a finite domain by choosing an upper limit of integration. The truncated tail may be easily controlled since the integrand is a bounded function multiplying a decaying exponential. We subsequently reduce the step size to resolve the oscillations arising from the cosine piece of the integrand. Second, this output is compared to that obtained through use of the NIntegrate function in *Mathematica.*

P. R. Kramer (private research notes) and Majda & Kramer (1999) also calculate the high Péclet number asymptotics for the integral in (5.1). They show that the enhanced diffusion term, $\kappa_{1,1}$, scales like $Pe^{2M/(M+1)}$ where M is the order of the largest order zero of the time-dependent component of the velocity. For our velocity, we have simple zeros, and therefore $M = 1$, giving a Pe^1 scaling for high Péclet numbers.

P. R. Kramer also derived an alternative integral representation for the same problem (private research notes). The first integral, given in (5.1), has an infinite limit of integration and, for high Pe values, can become extremely oscillatory. The alternative integral representation for the enhanced diffusion coefficient is a triple, as

https://doi.org/10.1017/S002211200100564X Published online by Cambridge University Press

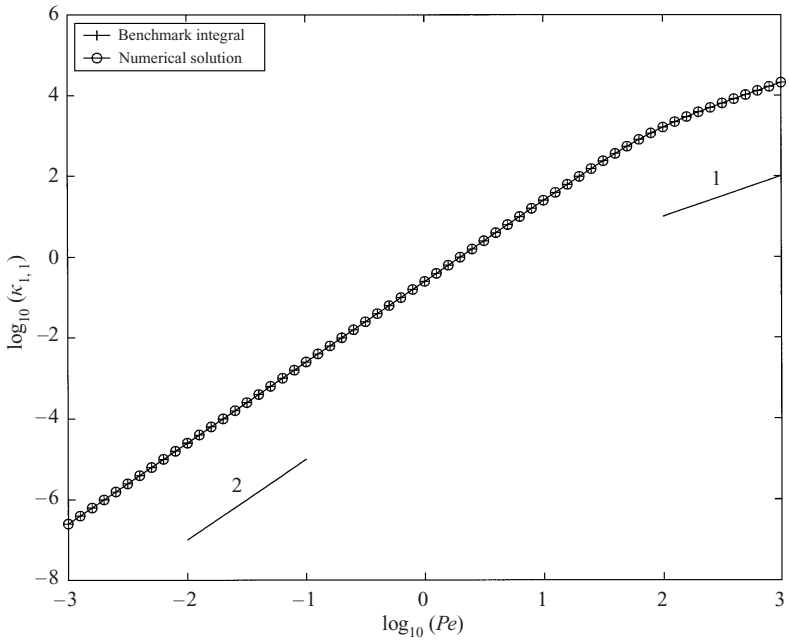


FIGURE 2. Benchmark of the conjugate gradient numerical technique compared with the numerical integration of (5.1). Both curves have the parameters $V_x = V_y = 0$ with $\delta_x = 0.1$ and $\delta_y = -0.05$. Also shown for reference are slope 1 and slope 2 lines.

opposed to double integral, over a finite domain, given by

$$\kappa_{1,1} = \frac{16\pi^4 Pe^2}{\tau_P} \int_0^{\tau_P} \left(\frac{\int_0^{\tau_P} \mu(1,\tau)\,\mathrm{d}\tau}{\mu(1,t)(\mu(1,\tau_P)-1)} + \frac{\int_0^t \mu(1,\tau)\,\mathrm{d}\tau}{\mu(1,t)} \right) \times \left(\frac{\int_0^{\tau_P} \mu(-1,\tau)\,\mathrm{d}\tau}{\mu(-1,t)(\mu(-1,\tau_P)-1)} + \frac{\int_0^t \mu(-1,\tau)\,\mathrm{d}\tau}{\mu(-1,t)} \right) \mathrm{d}t \qquad (5.2)$$

where $\mu(k,t)$ is an integrating factor for an ordinary differential equation in Fourier space, given by

$$\mu(k,t) = \exp\left(8\pi^2 k^2 t - 2\pi \mathrm{i} k\, Pe \left[\int_0^t (\delta_x - \delta_y) \sin\left(\frac{2\pi}{\tau_P} s \right) \mathrm{d}s + (V_x - V_y)t \right] \right).$$

This integral also must be tabulated numerically. This was accomplished using the NIntegrate function in *Mathematica*. Note that while this integral has finite limits of integration, it can still suffer from highly oscillatory behaviour for large enough Péclet numbers. In practice, the numerical quadrature of the integral (5.2) has fewer problems associated with oscillations than that in (5.1). The results from the numerical integration of (5.2) have been compared with the numerical quadratures for (5.1) and the results are indistinguishable.

Using these numerical quadratures, we turn now to the benchmarking of the conjugate gradient algorithm. For this benchmarking procedure, we study the situation

https://doi.org/10.1017/S002211200100564X Published online by Cambridge University Press

with $\tau_P \geqslant 1$. We first discuss the asymptotic regimes. At low Péclet number, the enhanced diffusion coefficients admit generically quadratic Péclet number scaling. Majda & Kramer have shown that at high Péclet number, the asymptotic scaling is linear in the Péclet number. As a benchmark, we demonstrate that the crossover connecting the low Péclet number asymptotics with the high Péclet number asymptotic scaling is precisely captured by the conjugate gradient algorithm. For the case when $\tau_P = 1$ this is shown in figure 2. This simulation is run in the absence of a mean wind, and with $\delta_x = 0.1$ and $\delta_y = -0.05$. Also notice that the scaling behaviour is accurate. That is, for small Pe, the scaling of the enhanced diffusion is like Pe^2, which holds for all situations. Also, for large Pe, the scaling behaves like Pe^1, which fits the asymptotic results shown in Majda & Kramer (1999). We comment that for larger values of τ_P, the enhanced diffusion coefficients show only a small change from the case with $\tau_P = 1$. Below, we demonstrate that the opposite limit, $\tau_P \to 0$, leads to dramatically different behaviour at high Péclet numbers (of the same order as presented in figure 2). The general limits for general topology will be addressed in the following section.

6. Results

We now turn to exploring new behaviour in the enhanced diffusion coefficients for the shear geometry, and then for cases with more complex topology, first with unsteady winds in two spatial dimensions, and then for the spatially three-dimensional ABC flow, with large-scale wind. We begin by presenting the various limiting analytical asymptotic calculations holding for general topology.

6.1. *Asymptotically small τ_P regime* (*large Strouhal number*)

We begin by examining the case where τ_P is small. First, the limit $\tau_P \to 0$ may be formally deduced easily using a multi-scale expansion for the general flow geometry studied here in (4.1). We relegate these calculations to the Appendix. The results demonstrate that for fixed Péclet number, the limit of vanishing time period should agree exactly with that of the steady cell problem, with the unsteady fluid flow being replaced by its temporal average. For the benchmark case, this should not be a surprise since, when looking at (5.1), letting τ_P approach zero has the same effect as letting $\delta_x = \delta_y = 0$. We see this result in figure 3 where we have results for the benchmark case where $\delta_x - \delta_y = 0.2$ for the three different values of $\tau_P = 1, 0.01, 0.001$. Now, the steady-state solution for similar parameter values has slope 2 on a log-log plot of the Péclet number against the enhanced diffusion coefficient. We see that as τ_P decreases in value, the closer the curve approaches the slope 2 curve at high Péclet numbers. In terms of the Strouhal number, S, for a fixed Péclet number, letting τ_P approach zero is identical to letting $S = 1/(Pe\,\tau_P)$ approach infinity. For the geometry studied here, the behaviour in the limiting cases with $S \to \infty$, or (as discussed below) $S \to 0$, is contrary to comments made by Avellaneda & Vergassola (1995) who remark that the steady-state behaviour is reproduced as S approaches zero. We study the limit of vanishing Strouhal number in the following subsection where we establish that in fact the enhanced diffusion coefficients for small Strouhal number are given by a particular average over the steady geometry. Observing that $S = 1/(Pe\,\tau_p)$, we remark that for fixed Péclet number, the steady geometry is obtained in the limit of infinite Strouhal number, and below we document that the limit of vanishing Strouhal number is quite subtle, and may be generally quite different than the steady geometry.

https://doi.org/10.1017/S002211200100564X Published online by Cambridge University Press

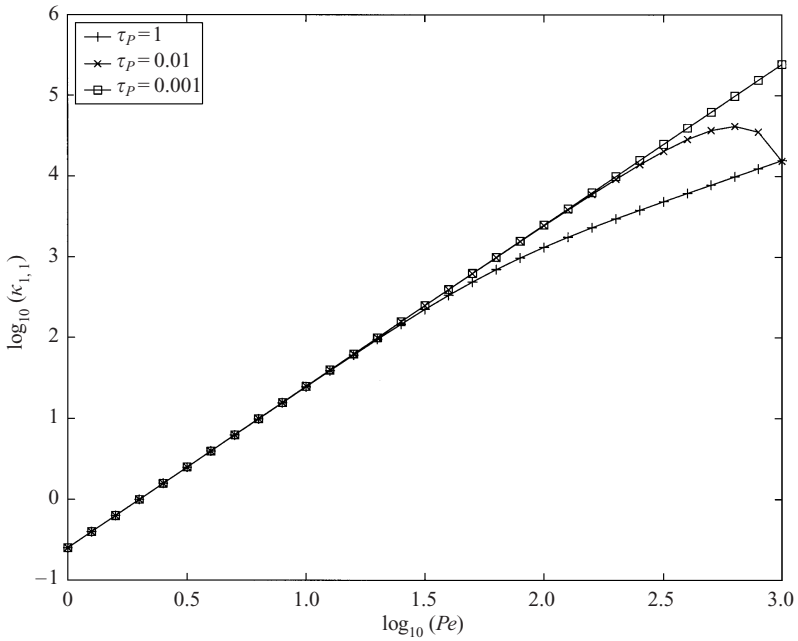


FIGURE 3. The effect of decreasing τ_P, the enhanced diffusion coefficients approach those of the steady-state case as seen in the benchmark case with $\delta_x - \delta_y = 0.2$.

Notice one other interesting feature shown in figure 3: in the case where $\tau_P = 0.01$, we observe a decrease in the enhanced diffusion coefficient as the Péclet number is increased from $10^{2.8}$ to 10^3, indicative of non-monotonic dependence upon the Péclet number. This reduction in enhanced diffusion has been verified by increasing the resolution of the numerical integration scheme and by using more Fourier modes in the conjugate gradient scheme. In fact, when the conjugate gradient scheme showed convergence using Fourier modes $n, m, l = -5, \ldots, 5$, we checked for artificial convergence by working with modes from $-100, \ldots, 100$ in all directions. This increase in resolution produced no change in the behaviour. Another interesting result is that if we calculate the curve for $\tau_P = 0.001$ for high enough Péclet numbers, near $Pe = 10^4$, a similar region of decreasing enhanced diffusion as a function of increasing Péclet number is observed. By examining the same set of flow parameters for many different values of τ_P, we observe for $500 \leqslant Pe \leqslant 1000$, that by decreasing τ_P, the dependence of the enhanced diffusion coefficients upon the Péclet number changes dramatically: for moderate values of τ_P, the closure coefficients exhibit entirely monotonic Péclet number dependence, whereas for smaller τ_P, the enhanced diffusions demonstrate non-monotonicity in the Péclet number. This is documented in the surface plot in figure 4. Once again, we study the benchmark integral (5.2) with $\delta_x - \delta_y = 0.2$. We use values of Pe as described above and values of τ_P ranging from 0.01 to 0.2. We have also observed this non-monotonic behaviour with non-shear flows ($\varepsilon \neq 1$), once again with small τ_P. We comment that non-monotonic enhanced diffusion coefficients as a flow parameter is varied have been observed previously in the context of fluctuating random shear layers (and attributed to resonances) (Castiglione *et al.* 1998). However, here, this behaviour is observed as a function of the Péclet number, and some discussion is merited regarding how this observation is not in contradiction

https://doi.org/10.1017/S002211200100564X Published online by Cambridge University Press

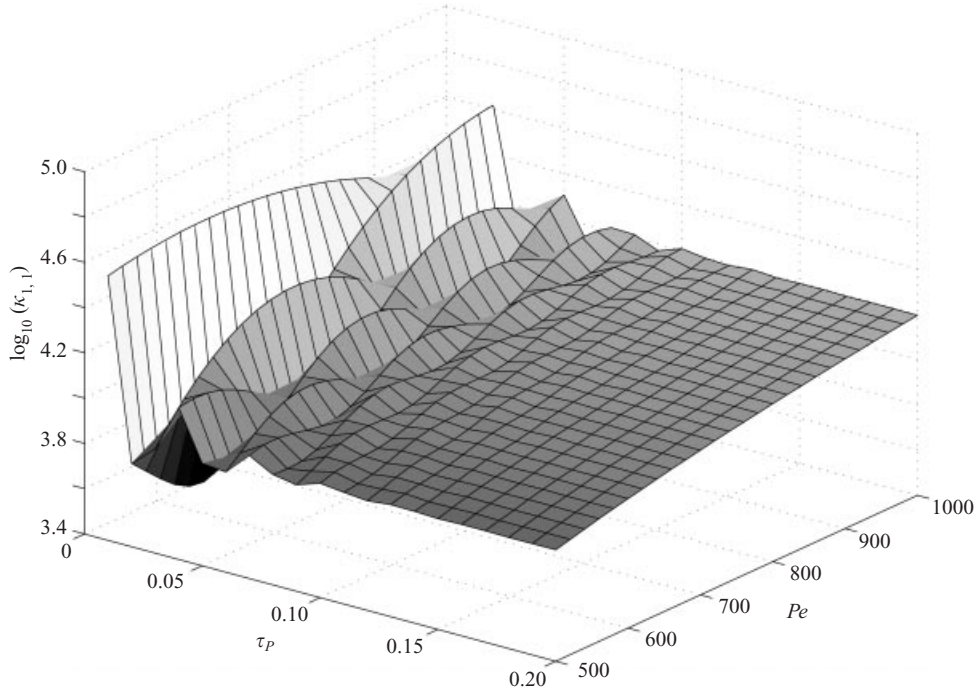


FIGURE 4. Surface plot of the integral (5.2) with $\delta_x - \delta_y = 0.2$ for $500 \leqslant Pe \leqslant 1000$ and $0.01 \leqslant \tau_P \leqslant 0.2$. Notice that as τ_P decreases, the enhanced diffusion coefficient becomes non-monotonic as a function of the Péclet number.

with the Stieltjes measure known to exist as a function of the Péclet number for fixed Strouhal number (Avellaneda & Vergassola 1995).

Avellaneda & Vergassola have shown that with the alternative non-dimensionalization discussed in § 2 (with Péclet and Strouhal numbers forming the independent non-dimensional parameters), the enhanced diffusion coefficients may be represented through a Stieltjes measure formula *as a function of the Péclet number*. The immediate ramification of this observation is that the enhanced diffusion coefficients must show monotonic dependence upon the Péclet number. We emphasize that in this case, the Stieltjes measure formula says nothing about the Strouhal number dependence. For the non-monotonic dependence just documented, we study the behaviour with the non-dimensional parameters (Pe, τ_P). In the light of the relation, $S = 1/(Pe\,\tau_P)$, we explore the effects of Strouhal numbers, $S = S(Pe)$. In the following subsection we explore a variety of Péclet-number-dependent Strouhal regimes which show the complexity of the joint limit $Pe \to \infty$, $S \to 0$. However, here, to demonstrate that our study properly reflects the Stieltjes measure formula, we re-draw the equivalent of figure 4, but as a function of (Pe, S). In figure 5, we calculate the enhanced diffusion coefficient through solutions to (5.2) with $\delta_x - \delta_y = 0.2$ and $500 \leqslant Pe \leqslant 1000$. Instead of changing values of τ_P, we now let S vary from 0.01 to 0.1. Observe that, along lines of constant S, the enhanced diffusion coefficient is monotonically increasing as a function of increasing Péclet number. However, notice that as Pe is held constant, we do not observe any monotonicity in terms of the Strouhal number. These subtle differences truly reflect differences in how the physical parameters are to be varied. Of course, these subtleties here are emerging at finite but large Péclet number, with small time period, $\tau_P = \tau_P(Pe) \ll 1$, in a regime where the incommensurate limits of

https://doi.org/10.1017/S002211200100564X Published online by Cambridge University Press

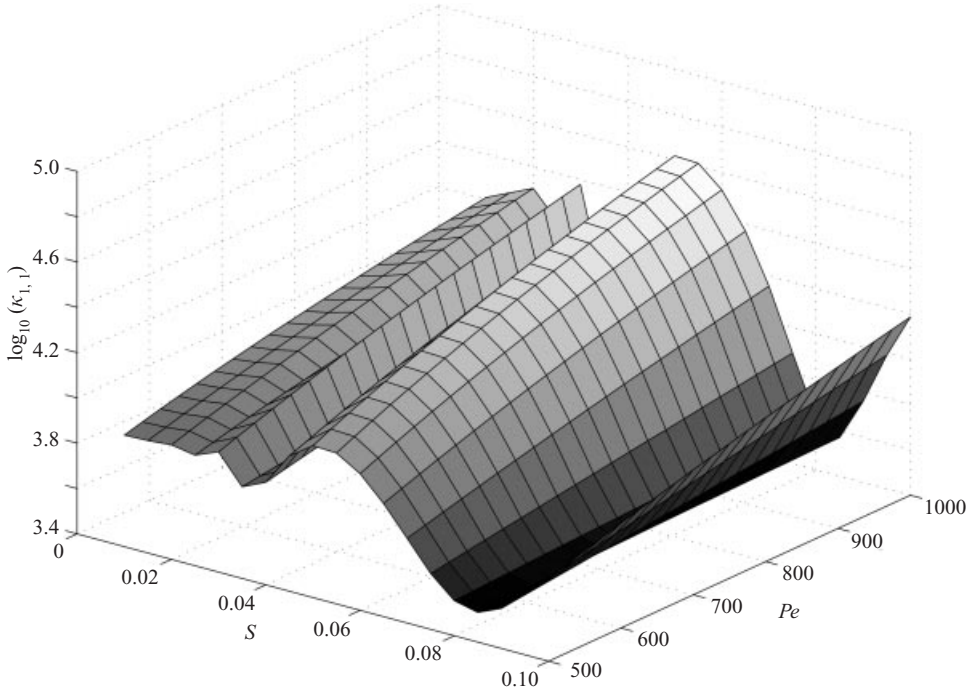


FIGURE 5. Surface plot of the integral (5.2) with $\delta_x - \delta_y = 0.2$ for values $500 \leqslant Pe \leqslant 1000$ and $0.01 \leqslant S \leqslant 0.1$. Notice that for constant S, the enhanced diffusion coefficient is monotonic in the Péclet number.

vanishing periodic Péclet number and infinite Péclet number are in proper balance. We remark that for cases involving non-sheared flows, with fixed $\tau_P \geqslant 1$, we always observe enhanced diffusions which are monotonic in the Péclet number, while similar non-monotonic scalings are observed for non-sheared topologies for cases with fixed $\tau_p \ll 1$.

6.2. *Asymptotically small Strouhal number regime* (*large* τ_p)

We next turn to considering the case of vanishing Strouhal number. To this end, it is most convenient to work with the non-dimensional group (Pe, S). In this non-dimensionalization, the temporally varying cell problem reads

$$S\,Pe\frac{\partial \Theta_j}{\partial t} + Pe(\boldsymbol{V} + \boldsymbol{v}(\boldsymbol{x}, t)) \cdot \nabla \Theta_j - \Delta \Theta_j = -Pe\,\boldsymbol{v}_j(\boldsymbol{x}, t) \tag{6.1}$$

where the temporal period is unity. In the present paper, we consider velocity fields of the form

$$\boldsymbol{v}(\boldsymbol{x}, t) = \boldsymbol{v}(\boldsymbol{x}) + \boldsymbol{A}(t)$$

for a temporally varying mean wind, $\boldsymbol{A}(t)$. The first thing to note is that the effect of the temporal variation in the driver above plays no role in the enhanced diffusion coefficients. This follows by observing the following separation of variables: Let

https://doi.org/10.1017/S002211200100564X Published online by Cambridge University Press

$\Theta_j(\boldsymbol{x},t) = \bar{\theta}_j(\boldsymbol{x},t) + M(t)$. Then $M(t)$ and $\bar{\theta}_j(\boldsymbol{x},t)$ satisfy

$$S\,Pe\frac{\partial \bar{\theta}_j}{\partial t} + Pe(\boldsymbol{V} + \boldsymbol{v}(\boldsymbol{x},t)) \cdot \nabla \bar{\theta}_j - \Delta \bar{\theta}_j = -Pe\,\boldsymbol{v}_j(\boldsymbol{x}),$$

$$S\,Pe\frac{\partial M}{\partial t} = -Pe\,\boldsymbol{A}_j(t).$$

So, $M(t)$ may be easily computed, but makes no contribution to the enhanced diffusivities as its spatial gradient vanishes identically.

Subsequently, the limit of vanishing Strouhal number is given by simply neglecting the time derivative in the equation for $\bar{\theta}_j$:

$$Pe(\boldsymbol{V} + \boldsymbol{A}(t) + \boldsymbol{v}(\boldsymbol{x})) \cdot \nabla \bar{\theta}_j - \Delta \bar{\theta}_j = -Pe\,\boldsymbol{v}_j(\boldsymbol{x}). \tag{6.2}$$

It should be stressed that this is not a singular limit due to the fact that this is a periodic boundary value problem, and not an evolution equation. Said differently, time and space are playing similar roles, and as such the highest-order derivative in this regard is the Laplacian. While somewhat formal at this stage, we remark that work in progress validates this approximation to be rigorously justifiable in the context of the periodic shear layer (Bonn *et al.* 2001).

It should be especially noted that in (6.2) the role of time is simply as a frozen coefficient in the equation. Therefore, the temporally varying portion of the wind, $\boldsymbol{A}(t)$, can be considered to be part of the constant mean, $\mathbf{V}$. We can then solve (6.2) as if it were a steady-state problem. Thus, we see that the enhanced diffusion coefficients are simply averages over the steady geometry by observing that the enhanced diffusions are spatio-temporal averages of gradients of $\bar{\theta}_j$:

$$\kappa_{i,j} = \int_0^1 \left(\int_{[0,1]^d} \nabla \bar{\theta}_i(\boldsymbol{x};t) \cdot \nabla \bar{\theta}_j(\boldsymbol{x};t)\,\mathrm{d}\boldsymbol{x} \right) \mathrm{d}t. \tag{6.3}$$

Noting that the expression in brackets is in fact the enhanced diffusion arising from the steady theory, with frozen time coefficient, we recognize that in the limit of vanishing Strouhal number, the enhanced diffusivities are given by an explicit average over the steady geometry.

Now it is worth commenting on the truly singular limit of large Péclet number, and its behaviour as the Strouhal number is varied. It is in this limit in purely steady flow that the enhanced diffusion coefficients were observed to admit a discontinuity supported upon a dense set of mean flow directions (Koch *et al.* 1989; Majda & McLaughlin 1993; Fannjiang & Papanicolaou 1994). We observe that for Péclet-number-dependent Strouhal numbers, we may expect, due to the singular nature of the large Péclet number limit, to observe quite complicated behaviour to exist as a function of both Péclet and Strouhal numbers, at finite, but large values of the Péclet number. To this end, we consider Péclet-number-dependent Strouhal numbers, $S = Q\,Pe^{-(1+\gamma)}$ for large values of the Péclet number. First, given the previous discussion, observe that as long as the product $(S\,Pe)$ vanishes in the limit of large Péclet number, we may expect that the time derivative has no effect, and may be similarly discarded as was done with fixed Péclet number. This will occur precisely when $\gamma > 0$. It should be stressed that this quite formal observation really should be supplemented by rigorous analysis. In work in progress, we are assessing the validity of this approximation for large Péclet number in the context of the time-varying shear layer (Bonn *et al.* 2001).

https://doi.org/10.1017/S002211200100564X Published online by Cambridge University Press

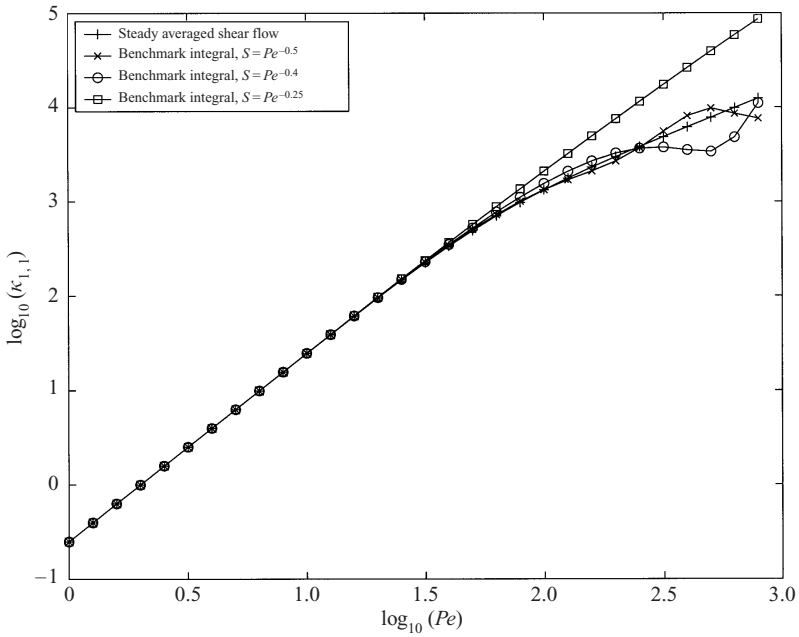


FIGURE 6. Enhanced diffusion coefficient in log-log coordinates for the time-varying shear profile with Péclet-number-dependent Strouhal number for $\gamma = -0.5, -0.6$ and -0.75. Notice that as γ decreases towards -1, the results deviate further from the average over the steady geometry. Here, $\delta_x - \delta_y = 0.2$.

We remark that numerical simulation presented in the following subsection documents numerically that this frozen time approximation is excellent for flows of general topology for $\gamma \geqslant 0$. It is somewhat remarkable, and not clear from inspection of the cell problem that this approximation works well even for $\gamma = 0$. However, for values of $\gamma < 0$, we next document that this approximation fails. Figure 6 shows the enhanced diffusion coefficient plotted in log-log coordinates as a function of the Péclet number for differing values of γ for the case of a sheared geometry, with flow parameters $\delta_x - \delta_y = 0.2$, $\varepsilon = 1$. Also included in this figure is the average over steady geometry given above in (6.3). Observe that the agreement between the steady average and the complete solution deteriorates as $\gamma < 0$ is decreased. This deterioration first appears as mild oscillation in the enhanced diffusion coefficient as a function of Péclet number for $\gamma = -0.5$. The amplitude of this oscillation grows as γ is further decreased, until ultimately, the oscillation vanishes (presumably being observed at larger Péclet numbers), saturating to the steady theory in this range of Péclet numbers as predicted by the asymptotic limit of infinite Strouhal number.

Figure 7 is a schematic phase diagram which summarizes these results. In the S vs. $1/Pe$ plane, we are mainly concerned with what happens near the singular point (the origin). The formal arguments in § 6.1 and § 6.2 suggest that the asymptotic behaviour of the enhanced diffusions depends upon the path of approach to the origin. The boundary separating fully unsteady phenomena from routine averaging of steady coefficients is the curve $S = 1/Pe$, shown in figure 7. Additionally, figure 7 depicts the behaviour at large Strouhal and finite Péclet numbers: fluctuation produces no modifications to the steady theory. We have cut out a neighbourhood of the origin to indicate that the precise asymptotic boundaries near this point are yet to be determined

https://doi.org/10.1017/S002211200100564X Published online by Cambridge University Press

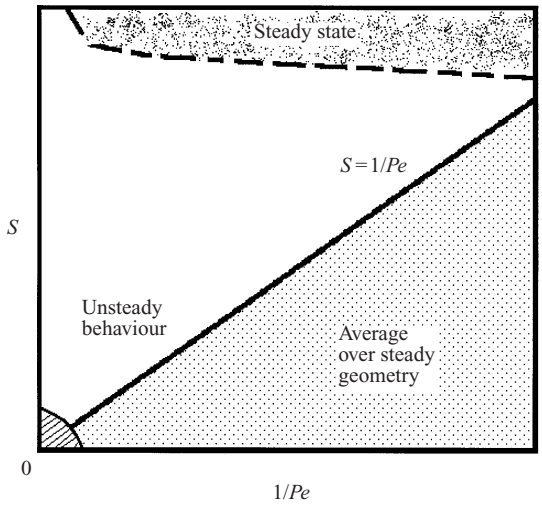


FIGURE 7. Schematic phase diagram of the S vs. $1/Pe$ plane. Near the origin, we expect the enhanced diffusion coefficients to be given as a routine average over the steady geometries when $S \leqslant 1/Pe$, while, for $S \geqslant 1/Pe$, fully unsteady theory prevails. When S approaches ∞, formal theory predicts fluctuations to not modify the steady theory.

generally. A more complete and rigorous description of the Péclet–Strouhal-number plane (including the origin) is being developed in current work (Bonn *et al.* 2001).

6.3. *Numerical results for non-sheared two-dimensional time-dependent flow*

We next turn to the study of how the sensitive Péclet number scaling, documented in the steady geometry (Majda & McLaughlin 1993) is modified through the incorporation of a temporally fluctuating large-scale mean wind for Strouhal number regimes in which temporal fluctuation may be expected to provide some averaging over the steady theory. Specifically, we focus upon the case, $S = Q/Pe$, ($\gamma = 0$), which is equivalent to fixing τ_P. This scaling is critical in separating behaviour given by a straight average over steady theory, and that arising from fully unsteady theory. As we argued in the previous section, this particular scaling is not governed by any obvious average over the steady geometry, whereas a straight average over the steady geometry will work for values of $\gamma > 0$. To explore $\gamma = 0$, we utilize our benchmarked conjugate gradient algorithm. We will document below that this case is indeed transitional: for $Q \leqslant 1$, the agreement between the fully unsteady theory agrees extremely well with the average over the steady geometry; however, for larger values of Q, the steady averaging fails, requiring fully unsteady theory.

We discussed the steady-state results earlier and they are illustrated in figure 1. Our purpose here will be to explore first how weak temporal fluctuation modifies the steady sensitive Péclet number scaling. This will be studied through consideration of how the addition of a small-amplitude fluttering mean wind modifies the predictions documented in figure 1. We will then turn to a discussion of larger-amplitude fluctuations.

In the simulations to follow, we consider the velocity field outlined in §4 and §6.2 with $\boldsymbol{V} + \boldsymbol{A}(t) + \boldsymbol{v}(\boldsymbol{x})$. $\boldsymbol{V}$ is a steady large-scale wind, $\boldsymbol{v}(\boldsymbol{x})$ is the background spatially varying flow field, and $\boldsymbol{A}(t)$ is the temporally fluctuating wind field. The flow parameters are given in (4.1), and we use the notation $\boldsymbol{V} = (V_x, V_y)^t$. We note that many of the calculations presented below for a fixed set of flow parameters, varying

https://doi.org/10.1017/S002211200100564X Published online by Cambridge University Press

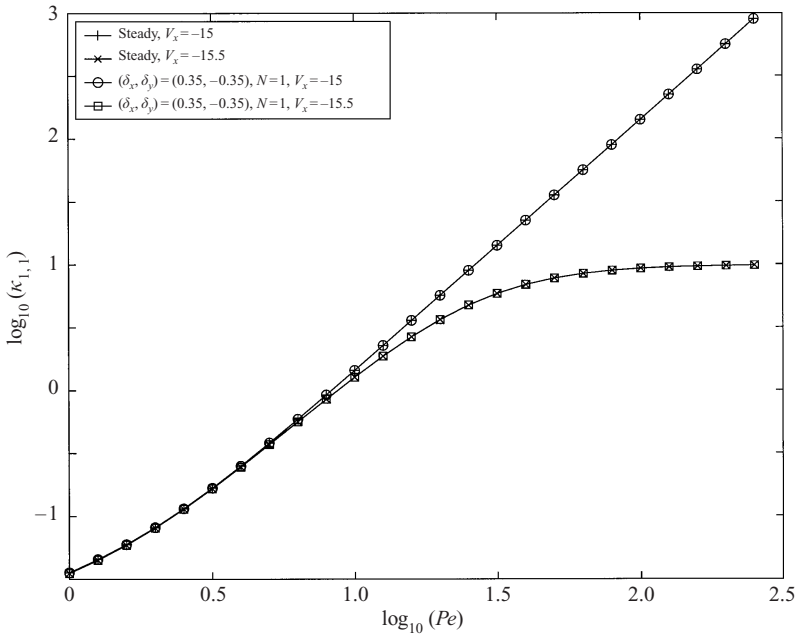


FIGURE 8. Example of a case with the fluctuating wind aligned with the steady wind. Both steady and $\delta_x = 0.35$, $\delta_y = -0.35$ cases are shown with $V_y = 15$ for all four curves.

only the Péclet number from 10^{-3} to $10^{2.4}$ in steps of 0.1 in logarithmic coordinates, consume 48 or more hours of wall clock time on the Dec Alpha 525 Mhz processor.

Unless stated otherwise, the results cited are with $\varepsilon = 0.5$. Similar numerical simulations with $\varepsilon = 0.1$ were performed, yielding qualitatively similar behaviour to that reported below. Also, the results cited are with $\phi = 0$ and $Q = 1$. Calculations with non-zero ϕ were performed, and significant differences were not observed, and similarly for the situation where $Q < 1$. In fact, performing simulations with $Q = 0.01$ produced less than a 0.01% change in the resulting enhanced diffusion coefficient with the parameters $\boldsymbol{V} = (-15, 15)$, $N = 1$, and $\delta_x = \delta_y = 0.2$. The enhanced diffusion coefficients are calculated utilizing the conjugate gradient algorithm described above, for various values of δ_x and δ_y both for $V_x = -15$ and $V_x = -15.5$, where $V_y = 15$. The orientation of the temporally fluttering mean wind is adjusted through the parameter, N. For cases where $N = 1$, the time-dependent component of the flow is always along a vector in the constant direction θ where $\tan(\theta) = \delta_y/\delta_x$. We additionally examined cases where $N = 2$, in which the frequency change gives a fluctuating wind field which changes direction throughout the period of the flow, $\tan(\theta) = 2\delta_y \cos(2\pi t)/\delta_x$. Simulations were further performed with $N = 3$ though no new behaviour was identified compared to the similar $N = 2$ case. The numerical runs break down into three cases:

Case 1: $N = 1$, $\delta_x = -\delta_y$. When $\delta_x = -\delta_y$, and $N = 1$, the direction of the time-dependent component of the flow is constant and parallel to the mean wind, $(-15, 15)^t$. There is little noticeable change in the behaviour of the enhanced diffusion coefficient. This should not be suprising since the time-dependent perturbation only affects the strength of the spatial mean of the flow at different times of the period, and not the direction. We illustrate this in figure 8 where we show the splitting achieved by the two runs $V_x = -15$ and $V_x = -15.5$ where in each run, $\delta_x = 0.35$

https://doi.org/10.1017/S002211200100564X Published online by Cambridge University Press

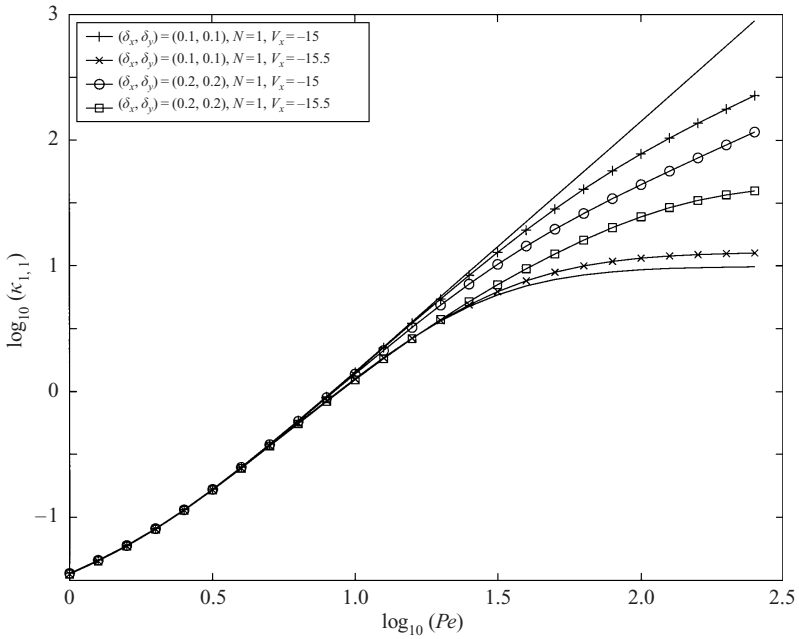


FIGURE 9. Two cases involving small-amplitude fluctuating wind perpendicular to the steady wind. The main cases break into: steady (the plain lines), $\delta_x = \delta_y = 0.1$ and $\delta_x = \delta_y = 0.2$, and all runs are done with $V_y = 15$. Notice that as we increase the magnitude of the perturbation, the splitting is less drastic.

and $\delta_y = -0.35$. Notice that not only does the splitting persist, but these two runs are actually superimposed on the steady runs with the same conditions and no change is noticeable.

Case 2: $N = 1$, $\delta_x = \delta_y$. In this case, the direction of the time-dependent perturbation is constant and perpendicular to the steady-state mean flow of $(-15, 15)^t$. In this case, we see more varied behaviour. As we increase the size of the perturbation from $\delta_x = \delta_y = 0$, we see that, while there still is a splitting between the $(V_x, V_y)^t = (-15, 15)^t$ and $(V_x, V_y)^t = (-15.5, 15)^t$ runs, the splitting is less dramatic as the amplitude of the perturbation increases. In fact, the splitting seems to 'zip up' as the amplitude increases. This is demonstrated in figure 9 where we show the steady cases, with $\delta_x = \delta_y = 0.1$ and $\delta_x = \delta_y = 0.2$.

We next briefly observe that the simpler tabulation of approximate enhanced diffusion emerging from the average over the steady geometry, given in (6.3), agrees in this case extremely well with the dynamic simulations. This is documented in figure 10. Here, we are interested in comparing the enhanced diffusions documented in figure 9 with those given by *steady averaging with a frozen time coefficient*. Additionally, we redraw the output from the unsteady calculations for the case with $\delta_x = \delta_y = 0.1$. Observe the striking agreement. However, we see next that with larger values of the constant Q, this agreement deteriorates as we effectively move into a different Strouhal number regime. This is documented in figure 11 where we compare the averaged enhanced diffusion coefficients arising from steady theory with those of the unsteady theory with $Q = 1$ and $Q = 20$. In all cases shown here, $V_x = -15$. For $Q = 1$, the agreement between steady averaging and the fully unsteady theory is excellent. However, the agreement is lost as Q is increased. Observe the difference between the averaged theory and the fully unsteady coefficients shown here with

https://doi.org/10.1017/S002211200100564X Published online by Cambridge University Press

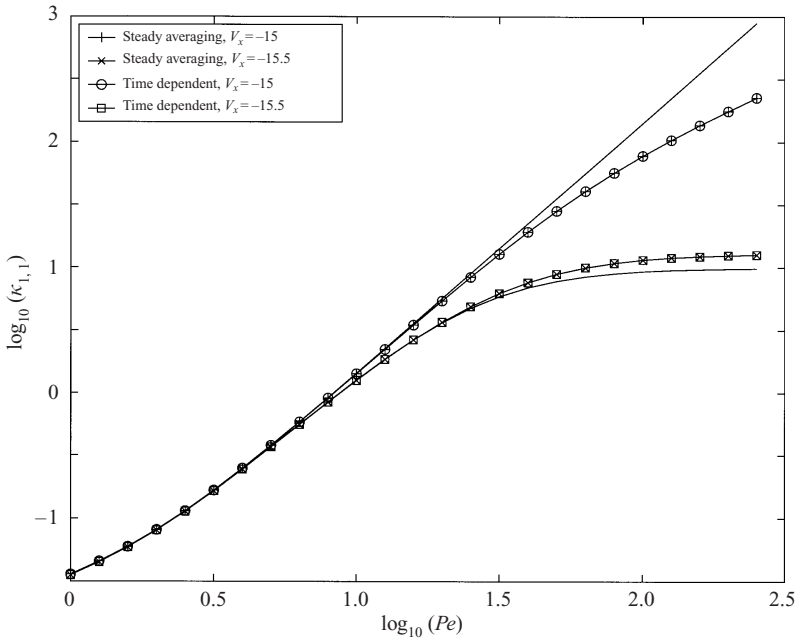


FIGURE 10. Comparison of enhanced diffusion coefficients given by averaging over steady geometries with fully unsteady calculations. For all simulations, $V_y = 15$, $\delta_x = \delta_y = 0.1$, and $Q = 1$. The outer curves (shown for reference) are the output of the purely steady (unaveraged) theory. Note that there is no visible difference between the averaged steady theory and the full simulation.

$Q = 20$. Consequently, the case with $\gamma = 0$ is indeed transitional. For negative values of γ, averages over the steady geometry will fail to be relevant, as seen below.

In the light of this delicacy regarding the success of steady averaging, we proceed henceforth utilizing the complete inversion of the unsteady cell problem. However, it is worth noting that for all cases we have studied, with $Q \leqslant 1$ and $\gamma \geqslant 0$, the frozen time approximation outlined in the previous subsection works exceptionally well.

Returning to the behaviour of the enhanced diffusion coefficients emerging from the complete inversion of the unsteady cell problem, we consider further increasing the amplitude of the fluctuating wind. For large-amplitude fluctuations (on the order of $\Delta \boldsymbol{V}$, the difference of the winds that exhibit large splittings, here (0.5, 0)), the presence of time fluctuations must somehow average the sensitive scaling existing in the steady geometry. This may be loosely explained simply because the distinct scaling identities, set by steady perturbation of the steady geometry, become in some sense 'statistically' identical in the presence of an additional, large-amplitude fluttering mean wind. Said differently, the distinct cases in the steady geometry with $\boldsymbol{V} = (-15, 15)$, and $\boldsymbol{V} = (-15.5, 15)$ produced dramatically different scalar mixing, are certainly less distinguishable when a large-amplitude temporally fluctuating mean wind is added, and should be expected to select, from the possible scalings arising for steady flow, some 'averaged' behaviour as a function of the Péclet number. Of course deducing what this averaged Péclet number dependence is, and if this averaging may be universal is both interesting and quite difficult. Recall, that Majda & Kramer (1999) have documented that the large Péclet number asymptotics for the shear layer with time-varying tranverse wind are set by the amount of time (the order of the zero of the temporally fluctuating transverse mean wind) this varying wind spends

https://doi.org/10.1017/S002211200100564X Published online by Cambridge University Press

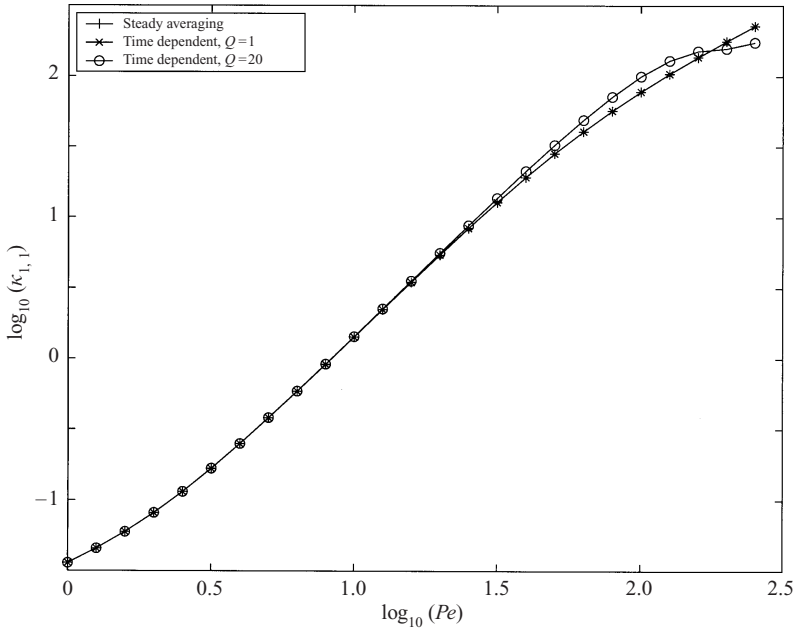


FIGURE 11. The results of the conjugate gradient calculation with $Q = 1$ and $Q = 20$ compared to the case of averaging over the steady geometry. For all simulations, $(V_x, V_y) = (-15, 15)$ and $\delta_x = \delta_y = 0.1$. Notice that as Q increases, the steady averaging fails.

in the vicinity of zero. This subtlety reflects the fact that in the shear geometry, it is the presence or absence of a steady tranverse wind which gives rise to dramatic change in the Péclet number scaling (Majda & McLaughlin 1993). In other words, in this flow geometry, there is a *single* value of the large-scale flow which dramatically modifies the transport properties. Observe that for flows with more general topology, the situation is much more complicated. The change in scaling is supported upon a dense set of flow directions (Koch *et al.* 1989; Majda & McLaughlin 1993; Fannjiang & Papanicolaou 1994). Clearly, the analogous study for more general topologies is not at present tractable. Nonetheless, we may begin to understand this temporal averaging through the study of temporal fluctuation involving only single Fourier modes.

As the size of the perturbation (δ) is increased, the sensitive Péclet number scaling is effectively smoothed by the temporal fluctuation. This is documented in figure 12, where $\delta_x = \delta_y = 0.65$. In this figure, we see that the splitting exhibited previously has been erased by the temporally varying component of the velocity. The enhanced diffusivities in the two cases are nearly parallel and close in value for sufficiently large Péclet numbers. Also notice that the slope of both curves in the log-log plot is nearly 1, indicating approximately linear scaling in the Péclet number. We stress that the degree of this smoothing strongly depends upon the particular Strouhal number regime: for $\gamma < 0$, this Pe^1 scaling is lost. In figure 13, we document several different values of γ: for $\gamma < 0$, the Pe^1 scaling is not observed. For such negative values of γ, the fully unsteady behaviour of the problem exhibits itself, even for large-scale fluctuations, as illustrated in figure 7. Recall that the formal theory presented in § 6.1 and § 6.2 suggests that routine averaging will work provided $\gamma > 0$.

https://doi.org/10.1017/S002211200100564X Published online by Cambridge University Press

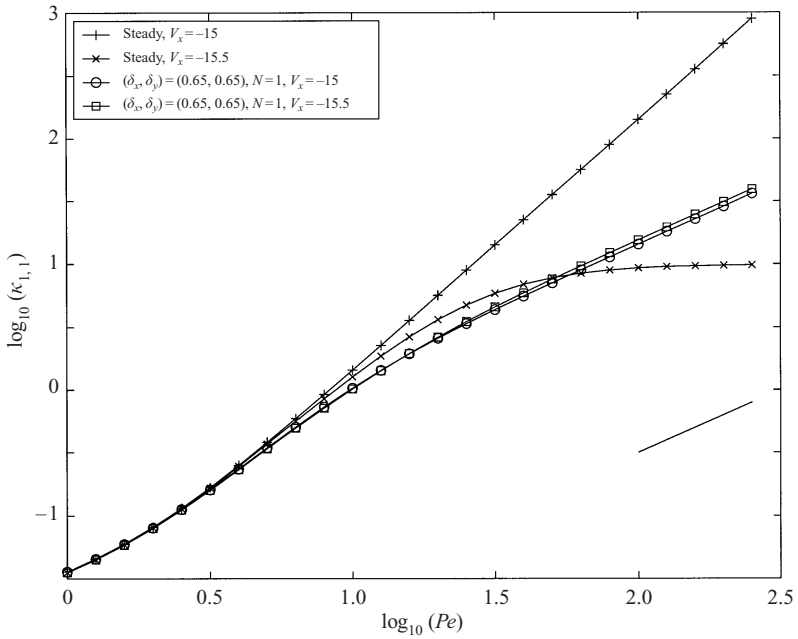


FIGURE 12. Further increased amplitude of fluctuating wind with $\delta_x = \delta_y = 0.65$. The splitting has been 'zipped up', in place of the averaged approximately linear (slope one line shown for reference) scaling behaviour. All simulations are with $V_y = 15$.

Case 3: $N = 2$, $\delta_x = \pm\delta_y$. When $N = 2$, the orientation of the fluctuating wind varies in time as $\tan(\theta) = \pm 2\cos(2\pi t)$. This change in direction affects the enhanced diffusion coefficient. Specifically, the degree of splitting between the enhanced diffusion coefficients corresponding to the different steady winds is reduced compared to case 1, but not as strongly as case 2. These observations are demonstrated in figure 14, where $N = 2$, with $\delta_x = 0.35$ and $\delta_y = -0.35$. Additionally depicted in figure 14 is the identical output corresponding to $\delta_x = \delta_y = 0.35$, and $N = 2$ (analogous to the cases with $N = 1$ documented in case 2). It should be noted that in further simulations, it has been seen that increasing the strength of the temporal fluctuation does not guarantee a reduction in the size of the relative splitting (Bonn 2001). This further emphasizes that while temporal fluctuation does aid in controlling the sensitive scaling occurring in the steady case, the precise details of this averaging are quite subtle and complicated, especially at fixed, finite Péclet number.

6.4. *Numerical results for three-dimensional steady flow*

We conclude with the calculation of the enhanced diffusion coefficients for a steady, but fully three-dimensional velocity field. Here we consider a background three-dimensional ABC flow, with the addition of a steady mean wind. Specifically, we consider an ABC velocity field given by

$$\boldsymbol{v}(x, y, z) = \begin{pmatrix} A\sin(z) + C\cos(y) + V_x \\ B\sin(x) + A\cos(z) + V_y \\ C\sin(y) + B\cos(x) + V_z \end{pmatrix}.$$

The purpose of this study is to document sensitive Péclet number scaling in the enhanced diffusion coefficients as the large-scale mean wind is varied. This sensitivity

https://doi.org/10.1017/S002211200100564X Published online by Cambridge University Press

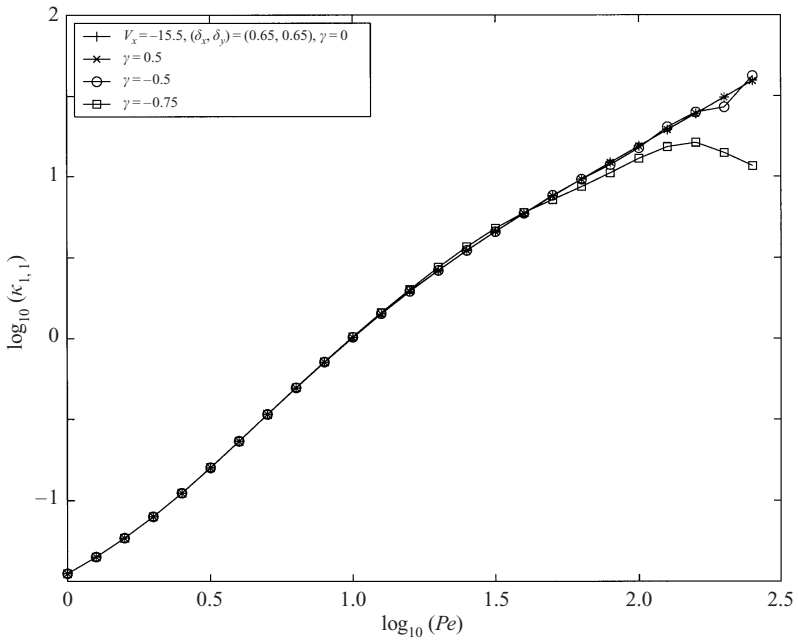


FIGURE 13. For $\gamma \geqslant 0$, slope 1 scaling exists for large enough fluctuations. (The curve for $\gamma = 0$ is the same as on figure 12.) For $\gamma < 0$, this scaling breaks for large values of Péclet number.

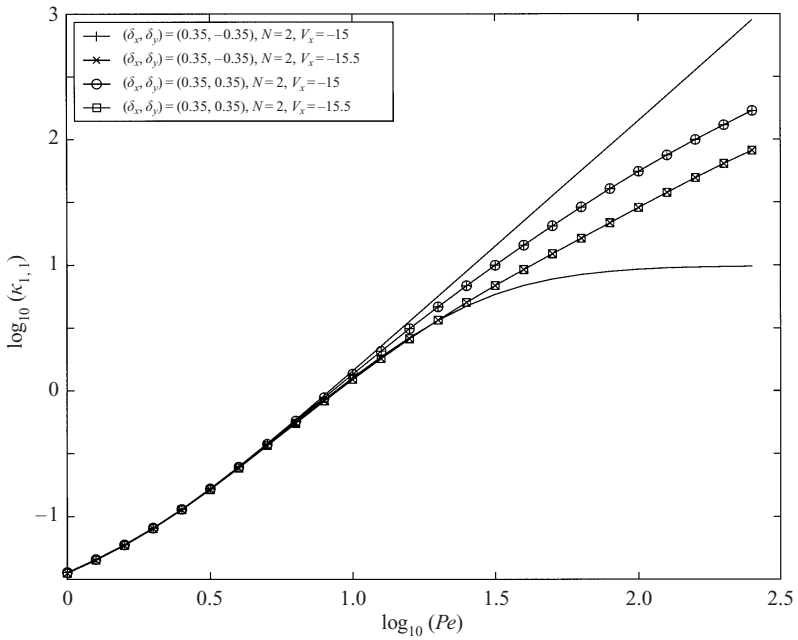


FIGURE 14. Enhanced diffusion for a case with an unsteady wind with dynamic orientation achieved by setting $N = 2$ (compare with the case where the fluctuating and steady wind fields are aligned parallel, figure 8 or perpendicular, figure 12).

is evidenced by a splitting in Péclet number scaling occurring at finite Péclet number. Using a similar numerical methodology to that documented in §4 (for numerical details consult Bonn 2001), we ran two simulations: one where $(V_x, V_y, V_z)^t = (5, 5, 5)^t$ and one where $(V_x, V_y, V_z)^t = (5.2, 5.05, 5)^t$. In both simulations, $A = B = C = 1$.

https://doi.org/10.1017/S002211200100564X Published online by Cambridge University Press

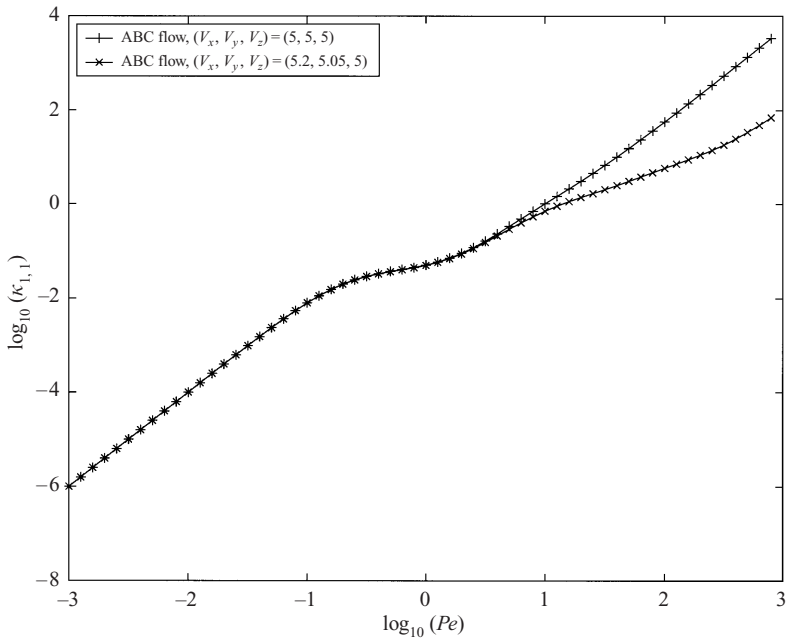


FIGURE 15. Two cases of the steady, three-dimensional, ABC flow. Both cases have $A = B = C = 1$. Notice the splitting in the enhanced diffusion coefficient scaling.

The numerical discretization is performed through a truncated Fourier spectral representation, and the same conjugate gradient iteration used in the latter sections is employed (Bonn 2001). The results are shown in figure 15. Notice that even though the x- and y-components of the wind are changed by only 4% and 1%, respectively, there is a strong change in Péclet number dependence of the enhanced diffusion. For the perturbed curve, there is an extended transition region where the slope in log-log coordinates is approximately 0.9 for a large number of Péclet number values, from about $Pe = 10^{1.2}$ to $Pe = 10^{2.2}$. And while the overall change is less dramatic than in the two-dimensional geometry, nonetheless, the addition of a spatial dimension does not remove the sensitivity of the enhanced diffusion coefficients to small perturbations in large-scale coefficients, at least at finite Péclet number.

7. Conclusions

We have presented an asymptotic and numerical study addressing how the introduction of temporal fluctuation modifies the complicated Péclet number scaling behaviour existing in homogenized eddy diffusion coefficients arising in two-dimensional steady flow with large-scale mean winds. The study is successful in identifying various Strouhal number regimes for which temporal fluctuation in the form of an additive time-varying wind may modify and average the poorly behaved steady theory, and Strouhal number regimes where temporal fluctuation leaves the steady theory either unchanged, or further complicated.

For Strouhal number regimes where fluctuation improves the steady enhanced diffusion coefficients (i.e. $S = Pe^{-(1+\gamma)}, \gamma \geqslant 0$), we utilized a conjugate gradient algorithm to explore the temporally averaged behaviour. We documented that for weak temporal fluctuations, the sensitivity in the enhanced diffusion coefficients is

https://doi.org/10.1017/S002211200100564X Published online by Cambridge University Press

smoother to some degree; however, the degree of smoothing is strongly dependent upon orientational details of the temporal fluctuation: for temporal fluctuations not strongly aligned with directions orthogonal to the background mean wind, little change in Péclet number dependence is noted, while fluctuations aligned strongly orthogonal to the background wind offer eddy diffusivities less sensitive to variation in large-scale flow properties. For large-amplitude fluctuations, strongly aligned with directions orthogonal to the background mean field, we observe that the sensitivity in the Péclet number scalings arising in steady theory is replaced by an effectively averaged enhanced diffusivity, scaling approximately as Pe^1. The present numerical study, while restricted to fluctuations involving only single Fourier modes, additionally documents that even if a universal asymptotic scaling law were possible in this Strouhal number regime, the mixing properties as a function of large-scale flow parameters at finite Péclet number are doubtless quite complex.

Perhaps more sophisticated mathematical theory can eventually be developed to address the quantitative and qualitative mixing properties of a passive scalar. Ultimately, methods need to be developed which can offer insight into the more difficult problems of understanding mixing properties in more realistic situations involving the incompressible Navier–Stokes equations, or even more complex issues associated with stratified mixing. Certainly, the present study illustrates just how difficult such an undertaking this may be.

R. M. M. acknowledges helpful discussions with D. Cai, R. Camassa, G. Forest, K. McLaughlin, D. W. McLaughlin, R. Pierrehumbert, R. Varadhan, A. Vulpiani, and W. Young, and thanks O. Pironneau for helpful discussions, and hospitality while visiting the Marie Curie University. Both authors acknowledge the helpful comments given by the reviewers; and Air Force Grant F49620-981-0501 for assistance in the purchase of the UNC Applied Mathematics Alphaserver. R. M. M. is partially supported by an NSF Career Grant, No. DMS-97019242; J. B. is partially supported by NSF Grant DMS-97004549.

Appendix. Perturbation calculation for $\tau_P \ll 1$

To see the behaviour of the enhanced diffusion coefficient for $\tau_P \ll 1$, we start with the cell problem, (3.5). Putting the velocity field into the cell problem, we have

$$\frac{\partial \Theta_j}{\partial t} - \Delta\Theta_j + Pe(\boldsymbol{v}(\boldsymbol{x}) + \boldsymbol{A}(t) + \boldsymbol{V}) \cdot \nabla\Theta_j = -Pe(v_j(\boldsymbol{x}) + A_j(t)).$$

We start with $\boldsymbol{v}(\boldsymbol{x})$ being periodic with period one and $\boldsymbol{A}(t)$ periodic with period τ_P. We rescale the time variable and let $\tau = t/\tau_P$. Substituting, we get the rescaled equation

$$\frac{\partial \Theta_j}{\partial \tau} - \tau_P \Delta\Theta_j + \tau_P\, Pe(\boldsymbol{v}(\boldsymbol{x}) + \boldsymbol{A}(\tau) + \boldsymbol{V}) \cdot \nabla\Theta_j = -\tau_P\, Pe(v_j(\boldsymbol{x}) + A_j(\tau)). \qquad \text{(A 1)}$$

In this rescaled cell problem, $\boldsymbol{A}(\tau)$ is periodic with period one. Therefore, the solution to (A 1) is periodic in space and time with period one. Assuming that $\tau_P \ll 1$, we expand the solution to (A 1) as a series in terms of the small parameter,

$$\Theta_j(\boldsymbol{x}, t) = \Theta_j^0(\boldsymbol{x}, t) + \tau_P \Theta_j^1(\boldsymbol{x}, t) + \tau_P^2 \Theta_j^2(\boldsymbol{x}, t) + \cdots . \qquad \text{(A 2)}$$

Substituting (A 2) into (A 1) and collecting terms of like powers of τ_P, the τ_P^0 and τ_P^1

https://doi.org/10.1017/S002211200100564X Published online by Cambridge University Press

equations, respectively, are

$$\frac{\partial \Theta_j^0}{\partial \tau} = 0, \tag{A 3}$$

$$\frac{\partial \Theta_j^1}{\partial \tau} = \Delta \Theta_j^0 - Pe(\boldsymbol{v}(\boldsymbol{x}) + \boldsymbol{A}(\tau) + \boldsymbol{V}) \cdot \nabla \Theta_j^0 - Pe(v_j(\boldsymbol{x}) + A_j(\tau)). \tag{A 4}$$

The leading-order term of the solution, Θ_j^0 depends only on $\boldsymbol{x}$ and is independent of τ. Also, the solution is periodic with period one and has zero mean.

We apply the Fredholm Alternative Theorem to determine existence of a solution to (A 4). Therefore, the right-hand side of (A 4) must be orthogonal to the null space of the adjoint of the operator on the left-hand side of the equation. The null space is spanned by functions $f(\boldsymbol{x})$ which have zero mean and are periodic in space with period one. A natural inner product to use is $(f, g) = \langle f \cdot g \rangle$ with $\langle \cdot \rangle$ as defined in (3.1). Therefore, we need, for all mean-zero, unit periodic functions $f(\boldsymbol{x})$,

$$\begin{aligned} 0 &= (\Delta \Theta_j^0 - Pe(\boldsymbol{v}(\boldsymbol{x}) + \boldsymbol{A}(\tau) + \boldsymbol{V}) \cdot \nabla \Theta_j^0 - Pe(v_j(\boldsymbol{x}) + A_j(\tau)), f(\boldsymbol{x})) \\ &= (\Delta \Theta_j^0 - Pe(\boldsymbol{v}(\boldsymbol{x}) + \boldsymbol{V}) \cdot \nabla \Theta_j^0 - Pe\, v_j(\boldsymbol{x}), f(\boldsymbol{x})) - Pe(\boldsymbol{A}(\tau) \cdot \nabla \Theta_j^0 + A_j(\tau), f(\boldsymbol{x})) \\ &= (\Delta \Theta_j^0 - Pe(\boldsymbol{v}(\boldsymbol{x}) + \boldsymbol{V}) \cdot \nabla \Theta_j^0 - Pe\, v_j(\boldsymbol{x}), f(\boldsymbol{x})) \end{aligned} \tag{A 5}$$

since

$$\begin{aligned} (\boldsymbol{A}(\tau) \cdot \nabla \Theta_j^0 + A_j(\tau), f(\boldsymbol{x})) &= \int_0^1 \int_0^1 \int_0^1 (\boldsymbol{A}(\tau) \cdot \nabla \Theta_j^0 + A_j(\tau)) f(\boldsymbol{x})\, \mathrm{d}x\, \mathrm{d}y\, \mathrm{d}\tau \\ &= \int_0^1 \int_0^1 f(\boldsymbol{x}) \left[\nabla \Theta_j^0 \cdot \left(\int_0^1 \boldsymbol{A}(\tau)\, \mathrm{d}\tau \right) \right. \\ &\quad \left. + \int_0^1 A_j(\tau)\, \mathrm{d}\tau \right] \mathrm{d}x\, \mathrm{d}y = 0 \end{aligned}$$

since $\boldsymbol{A}(\tau)$ has zero mean.

Equation (A 5) gives a condition on Θ_j^0 for the solvability of Θ_j^1. Since Θ_j^0 has zero mean and is periodic with period one, $\Delta \Theta_j^0 - Pe(\boldsymbol{v}(\boldsymbol{x}) + \boldsymbol{V}) \cdot \nabla \Theta_j^0 - Pe\, v_j(\boldsymbol{x})$ is also mean zero with period one. Thus, for the inner product (A 5) to be zero for all appropriate choices of $f(\boldsymbol{x})$, it is necessary that

$$\Delta \Theta_j^0 - Pe(\boldsymbol{v}(\boldsymbol{x}) + \boldsymbol{V}) \cdot \nabla \Theta_j^0 - Pe\, v_j(\boldsymbol{x}) = 0$$

which is precisely the equation of the steady-state cell problem.

Therefore, the leading-order term of the perturbation expansion is the solution to the steady-state cell problem.

REFERENCES

Avellaneda, M. & Majda, A. J. 1991 An integral representation and bounds on the effective diffusivity in passive advection by laminar and turbulent flows. *Commun. Math. Phys.* **138**, 339–391.

Avellaneda, M. & Vergassola, M. 1995 Stieltjes integral representation of effective diffusivities in time-dependent flows. *Phys. Rev.* E **52**, 3249–3251.

Batchelor, G. K. 1967 *An Introduction to Fluid Dynamics.* Cambridge University Press.

Bensoussan, A., Lions, J. L. & Papanicolaou, G. 1978 *Asymptotic Analysis for Periodic Structures.* North-Holland-Elsevier.

https://doi.org/10.1017/S002211200100564X Published online by Cambridge University Press

Bonn, J. 2001 Advective diffusion in the presence of idealized turbulence. PhD Dissertation, University of North Carolina, in preparation.

Bonn, J., Camassa, R., McLaughlin, K. T. R. & McLaughlin, R. M. 2001 Rigorous Strouhal–Péclet enhanced diffusion asymptotics for the time-varying shear layer. In preparation.

Brenner, H. & Edwards, D. A. 1993 *Macrotransport Processes*. Butterworth-Heinemann.

Castiglione, P. 2000 Diffusion coefficients as function of Kubo number in random fields. *J. Phys.* A: *Math. Gen.* **33**, 1975–1986.

Castiglione, P., Crisanti, A., Mazzino, A., Vergassola, M. & Vulpiani, A. 1998 Resonant enhanced diffusion in time-dependent flow. *J. Phys.* A: *Math. Gen.* **31**, 7197–7210.

Concus, P. & Golub, G. H. 1976 A generalized conjugate gradient method for nonsymmetric systems of linear equations. In *Computing Methods in Applied Sciences and Engineering* (ed. R. Glowinski & J. L. Lions). Lecture Notes in Economics and Mathematical Systems, vol. 134, pp. 56–65. Springer.

Crisanti, A., Falcioni, M., Paladin, G. & Vulpiani, A. 1990 Anisotropic diffusion in fluids with steady periodic velocity fields. *J. Phys.* A: *Math. Gen.* **23**, 3307–3315.

Fannjiang, A. & Papanicolaou, G. 1994 Convection enhanced diffusion for periodic flows. *SIAM J. Appl. Maths* **54**, 333–408.

Knobloch, E. & Merryfield, W. J. 1992 Enhancement of diffusive transport in oscillatory flows. *Astrophys. J.* **401**, 196–205.

Koch, D. L. & Brady, J. F. 1989 Anomalous diffusion due to long-range velocity fluctuations in the absence of a mean flow. *Phys. Fluids* A **1**, 47–51.

Koch, D. L., Cox, R. G., Brenner, H. & Brady, J. F. 1989 The effect of order on dispersion in porous media. *J. Fluid Mech.* **200**, 173–188.

Landau, L. 1944 *Dokl. Acad. Sci. URSS* **43**, 286.

Landau, L. & Lifshitz, E. 1987 *Fluid Mechanics*. Pergamon Press.

Majda, A. J. 1990 Lecture Notes on Turbulent Diffusion, Graduate Course, Princeton University.

Majda, A. J. & Kramer, P. R. 1999 Simplified models for turbulent diffusion: Theory, numerical modelling, and physical phenomena. *Phys. Rep.* **314**, 237–574.

Majda, A. J. & McLaughlin, R. M. 1993 The effect of mean flows on enhanced diffusivity in transport by incompressible periodic velocity fields. *Stud. Appl. Maths* **89**, 245–279.

McCarty, P. & Horsthemke, W. 1988 Effective diffusion coefficient for steady two-dimensional convective flow. *Phys. Rev.* A **37**, 2112–2117.

McLaughlin, D., Papanicolaou, G. & Pironneau, O. 1985 Convection of microstructure and related problems. *SIAM J. Appl. Maths* **45**, 780–797.

McLaughlin, R. M. 1994 Turbulent transport. PhD Thesis, Program in Applied Computational Mathematics, Princeton University.

McLaughlin, R. M. 1998 Numerical averaging and fast homogenization. *J. Statist. Phys.* **90**, 597–626.

Mezic, I., Brady, J. F. & Wiggins, S. 1996 Maximal effective diffusivity for time-periodic incompressible fluid flows. *SIAM J. Appl. Maths* **56**, 40–56.

Moffatt, H. K. 1983 Transport effects associated with turbulence with particular attention to the influence of helicity. *Rep. Prog. Phys.* **46**, 621–664.

Ottaviani, M. 1992 Scaling laws of test particle transport in two-dimensional turbulence. *Europhys. Lett.* **64**, 4.

Pomeau, Y. 1985 Dispersion dans un ecoulement en presence de zones de recirculation. *C. R. Acad. Sci. Paris* **301**(II), 1323–1326.

Solomon, T. H. & Gollub, J. P. 1988 Passive transport in steady Rayleigh-Bernard convection. *Phys. Fluids* **31**, 1372–1379.

Young, W., Pumir, A. & Pomeau, Y. 1989 Anamolous diffusion of tracer in convection rolls. *Phys. Fluids* A **1**, 462–469.

https://doi.org/10.1017/S002211200100564X Published online by Cambridge University Press